NSK Technical Journal

Motion & Control

No. 23 June 2013

ISSN1342-3630

NSK

MOTION & CONTROL No. 23
NSK Technical Journal
Printed and Published: June 2013
ISSN1342-3630
Publisher: NSK Ltd., Ohsaki, Shinagawa, Tokyo, JAPAN
Public Relations Department
TEL +81-3-3779-7051
FAX +81-3-3779-7431
Editor: Naoki MITSUE
Managing Editor: Hitoshi EBISAWA
Design, Typesetting & Printing: Kuge Printing Co., Ltd.

NSK Technical Journal
Motion & Control
No. 23
June 2013

NSK

Contents

Technical Articles

New Products

Temperature Rise Analysis in Traction Contact Areas of Toroidal CVTs

—Influence of Half-Cone Angle on Temperature Rise

Shinji Miyata
Corporate Research & Development Center
Bernd-Robert Höhn and Klaus Michaelis
Technical University of Munich, Gear Research Centre (FZG)
Oliver Kreil
Technical University of Munich, Gear Research Centre (FZG) (Present affiliation: AGCO GmbH)

ABSTRACT

The toroidal traction-drive CVT transmits power by the shearing action of lubricant film under heavy loads at the contact ellipse on the rollers. Furthermore, due to the geometry of the toroidal CVT, spin motion is produced in the contact ellipse. These contact ellipses are where shear stress of the lubricant generates frictional heat. In this report, temperature rise in the traction contact areas of toroidal CVTs were analyzed using a traction analysis program after measuring temperature rise with a twin-disc test machine and comparing experimental results with calculated results. The influences of half-cone angles on temperature rise were discussed.

Translated and reprinted with permission from JSAE Transactions, Vol. 40, No. 2, March 2009

1. Introduction

Toroidal-type, continuously variable transmissions (CVTs) for use in large automobiles can be classified according to the intersecting angle of the normal axis on the tangent plane at the traction point of the power roller with in relation to the rotational axis of the roller (half-cone angle: θ_0): one is the half-toroidal type CVT with a half-cone angle of 62.5 degrees (as an example), and the other is a full-toroidal variator with a half-cone angle of 90 degrees (see Figure 1). In the half-toroidal variator, heat generation in the contact area is considered to be small because the amount of spin that is generated by geometric configuration of toroid in the contact area is small, while heat generation in the full-toroidal variator is considered to be large because the amount of spin in the contact area is large, though heat generation occurs by shearing of oil film in the traction contact area [1]. However, such hypotheses regarding heat generation have been only been discussed in theory, while quantitative values of temperature rise are lacking, and the influence of the half-cone angles on temperature rise have not been clarified until now.

Meanwhile, it is known that the maximum traction coefficient decreases under conditions of high oil temperatures [2]. Temperature rise in the traction contact area is naturally considered to have a close relationship with the traction coefficient. Therefore, clarifying temperature rise in the traction contact area for predicting the traction coefficient with more precision becomes necessary.

A considerable amount of research regarding characteristics of the traction contact area has been conducted in the past. In theory, Dowson [3] et al. or Taniguchi [4] et al. clarified the influence of spin on oil film thickness, while Johnson [5] et al. proposed a viscoelastic model to reasonably explain traction characteristics. In recent years, a traction analysis model [1), 6)] that takes into consideration the amount of heat generation in the contact area has been developed, thus enabling use of the traction coefficient for making predictions to some extent. Although oil temperature [7), 8)] or bulk temperature [9)] has been measured in actual CVT test rigs in regards to temperature rise, however, temperature rise in the traction contact area that takes into consideration spin motion has not been clarified experimentally due to the difficulty of measuring temperature rise in the contact area directly, and due to temperature rise analysis results in the contact area having not been verified.

For the first time, the authors measured and clarified the amount of temperature rise in the contact area under high-speed rolling conditions with spin motion in a minute sliding area that are typically found in a toroidal CVT, using twin-disc test machine [10)]. This report shows that it is now possible to predict temperature rise in the traction contact area while considering the calculated influence of spin, comparing measured results of temperature rise in the traction contact area with the calculated results using a traction analysis program, which takes into consideration the amount of heat generation, that was developed at the Technical University of Munich. Additionally, this report presents results that clarify the influence of the half-cone angle on temperature rise by analyzing temperature rise in the traction contact area of a half-toroidal variator and full-toroidal variator using the aforementioned traction analysis program.

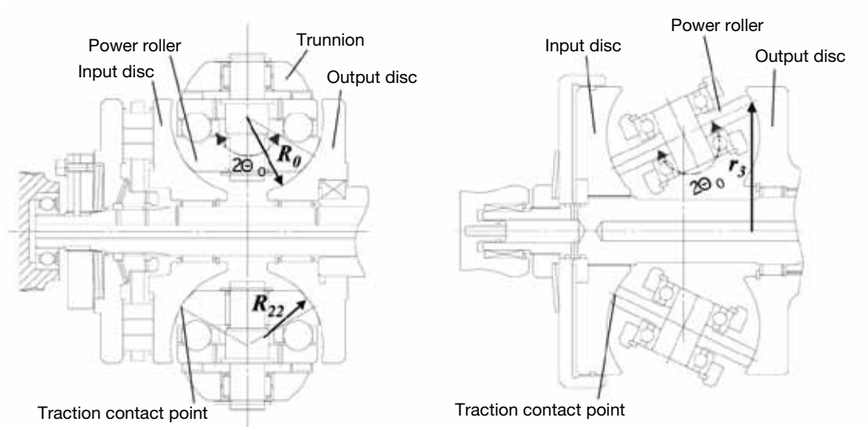

Fig. 1 Half-toroidal (left) and full-toroidal CVT (right)

2. Measured Results of Temperature Rise in Traction Contact Area

A twin-disc test machine (Figure 2) was used for measuring temperature rise in the traction contact area. Each disc was independently driven so that any desired slip ratio can be achieved. Measurements were taken using the disc combinations illustrated in figure 3 under conditions of spin and no-spin using a conic disc with a half cone angle (α). Table 1 lists ratios between the spin angular velocity, ω_{SP}, and disc angular velocity, ω_1, When comparing values of temperature rise under conditions of spin and no-spin, disc combinations of A2 and B had the same radius R. A thin-film platinum temperature sensor (see Figure 4) was sputtered on the cylindrical and conic discs. The thin film sensors run directly over the traction contact surface where electrical resistance of the platinum changes with pressure and temperature. Distribution of temperature rise was thus measured in the contact areas by measuring changes in electrical resistance. Measurements have a margin of error of ±8 percentage points. Reference 10 presents details of the measuring methodology.

The solid lines in Figure 5 (a) show measured results of temperature distribution in the elliptical contact areas for varying degrees of slip ratio under no-spin conditions. The horizontal axis shows the dimensionless position in the rolling direction. The temperature increased rapidly according to rise in pressure after passing the inlet zone and follows the same pattern as pressure distribution. After passing the center of the contact point, the temperature continued to increase slightly and then tapered off. After which, a second temperature peak can be seen. In addition, it was experimentally confirmed that as the slip ratio increased, the level of temperature distributions also increased. The measured results (solid line) of the same temperature rise distribution could be

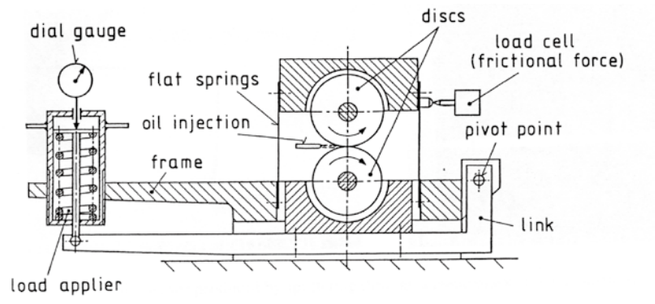

Fig. 2 Twin-disc test machine

obtained under conditions of spin motion (Figure 5 (b)).

Figure 6 shows measured results of the influence of spin and no-spin on the maximum temperature rise. Disc combinations of A2 and B were used with the same radius of R for comparing the influence of spin and no-spin conditions. The maximum temperature rise under conditions of spin was higher than that under conditions of no-spin as shown in Figure 6 (a). Temperature differences that were generated between spin motion and no-spin motion decreased as the slip ratio increased. Figure 6 (b) shows the ratio of measured results of maximum temperature rise under conditions of spin and no-spin (solid line). The ratio was approximately 1.3 at a slip ratio of 0 %, but reached close to 1 as the slip ratio increased. It was determined that the influence of spin motion on temperature rise was large in the lower area of the slip ratio and that the influence of spin motion on temperature rise was small in the high area of slip ratio. Additionally it was found that an influence of a 1 % increase of slip ratio on temperature rise, for instance, is higher than that of existing spin motion on temperature rise.

Table 1 Specifications of disc combinations

	Without spin		With spin
Disc combination	A1	A2	B
Half cone angle, α (deg)	0		30
Spin ratio, ω_{sp}/ω_1	0		0.58
Lower disc radius, R (mm)	R20	R10	R10

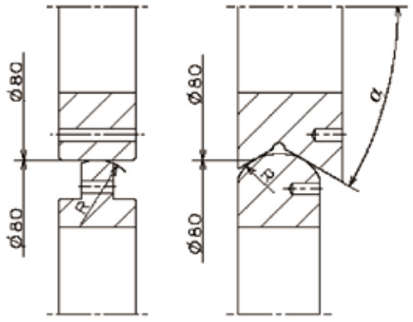

(a) Without spin (b) With spin

Fig. 3 Disc combinations

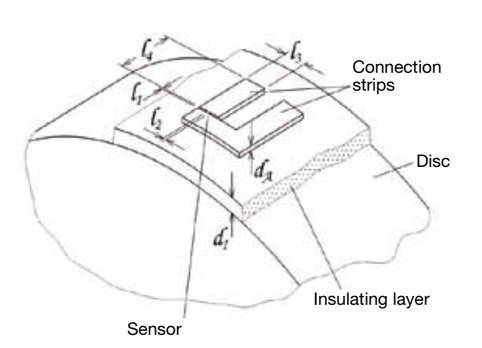

Fig. 4 Thin film sensor for temperature measurements

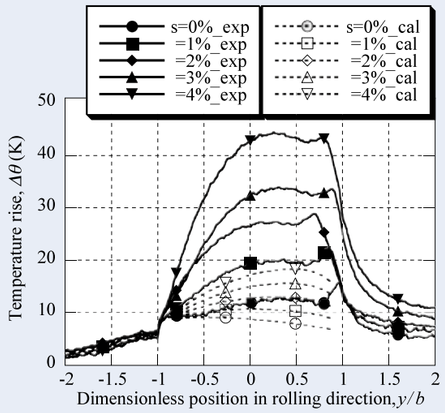

(a) With spin (Disc combination A1)

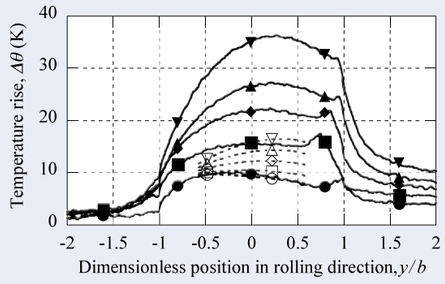

(b) Without spin (Disc combination B)

Fig. 5 Temperature rise in the traction contact surface of measurements (solid lines) and calculations (broken lines) (P = 980 MPa; v_1 = 12 m/s; θ_{oil} = 50 °C; θ_M = 50 °C)

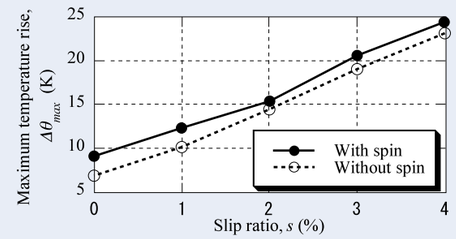

(a) Maximum temperature rise in the traction contact surface of measurements with spin motion (solid line) and without spin motion (broken line)

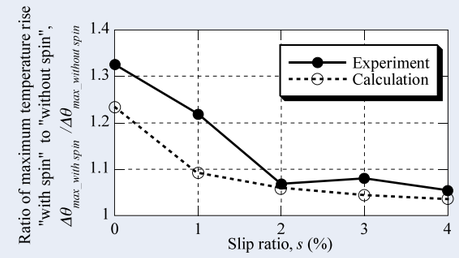

(b) Ratio of maximum temperature rise between "with spin motion" and "without spin motion" of measurements (solid line) and calculations (broken line)

Fig. 6 Influence of spin motion on temperature rise (P = 1 260 MPa; v_1 = 5 m/s; θ_{oil} = 50 °C; θ_M = 50 °C; Disc combination A2 and B)

3. Comparison with Analysis Results

3.1 Analysis program

A traction analysis program (REIB99)[6] that was developed at the Gear Research Centre (FZG) of the Technical University of Munich was used to calculate temperature distributions in the contact area. This program used a rheological model having viscoelastic characteristics as shown in equation (1), used another rheological model as shown in equation (2), and calculated temperature rise using the flash temperature theory[11]. (Refer to reference 6 for details.)

$$\dot{\gamma} = \frac{1}{G}\frac{d\tau}{dt} + \frac{\tau_0}{\eta}\sinh\left(\frac{\tau}{\tau_0}\right) \qquad (1)$$

$$\tau = \begin{cases} G_e\gamma & for \quad \gamma < \dfrac{\tau_p}{G_e} \\ \tau_p & for \quad \gamma \geq \dfrac{\tau_p}{G_e} \end{cases} \qquad (2)$$

where γ is shearing rate, G is modulus of transverse elasticity in the area of viscoelastic body, τ is shearing stress, τ_0 is Eyring stress, η is viscosity, G_e is modulus of transverse elasticity in the area of elasto-plastic body, and τ_p is limited shearing stress.

3.2 Comparisons between the calculations and measurements

The broken lines in Figure 5 show the calculated temperature distribution. After passing the center of the contact surface, the temperature increased and reached its maximum value where after it decreased. Although there was no second peak because theoretical Hertz pressure was used for calculation, characteristics of calculated results were qualitatively in good agreement with measured results.

Figure 7 shows the ratio between measured maximum temperature and calculated maximum temperature. Even if circumferential velocity v_1 and slip ratio s were changed, measured temperatures were approximately two times higher than the calculated temperatures. Even if surface pressure P was changed, notwithstanding spin conditions, the ratio was approximately twofold under the same measured conditions as shown in Figure 8. At the present moment, although both measured and calculated results have been confirmed as being valid, the difference between

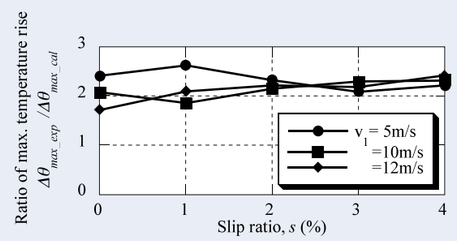

Fig. 7 Ratio of maximum temperature rise between experiments and calculations for different slip ratio and circumferential velocity (P = 980 MPa; θ_{oil} = 50 °C; θ_M = 50 °C; Disc combination A1)

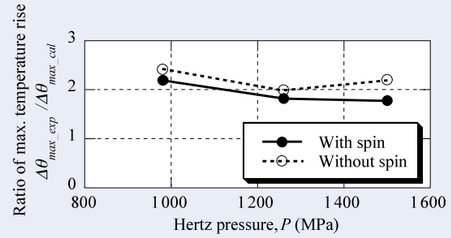

Fig. 8 Ratio of maximum temperature rise between experiments and calculations for different pressure with spin and without spin conditions (v_1 = 12 m/s; s = 4 %; θ_{oil} = 50°C; θ_M = 50°C; Disc combination A1 and B)

both results cannot be explained. This subject will be considered for future research.

In addition, Figure 6(b) shows the ratio (broken line) between measured maximum temperature and calculated maximum temperature under spin and no-spin conditions. Measured results and calculated results agreed well. Therefore, it seems reasonable to consider that the influence of spin on temperature rise could be considered.

As stated above, measurements and calculations showed good qualitative agreement notwithstanding the existence of spin motion. Measured temperatures were two times higher than the calculated temperatures under any condition in the experimental range. Therefore, it seems reasonable that the traction analysis program, REIB99, can simulate the tendency of temperature rise on the contact surface. Since the difference between measured and calculated values cannot be explained at the present moment, the correction factor of 2.0 was not applied in the calculations discussed in section 4 or later.

4. Analysis Results of Temperature Rise in Toroidal Variators

4.1 Comparison between half-toroidal and full-toroidal variators

Calculated results for temperature rise in the traction contact surface areas of the full- and half-toroidal variators were calculated using the above verified traction analysis program. Calculations were made for temperature rise distributions on the contact surface of the input discs for both of the half-toroidal and full-toroidal variators, which had nearly identical specifications as those listed in Table 2. Traction coefficient, maximum input torque, maximum input speed, and variator reduction ratio i_V (input angular velocity / output angular velocity) were the same for both variators. Radius of rotation to contact point of the output disc, r_3, of the full-toroidal variator was larger than that of the half-toroidal variator. However, the width of the half-toroidal variator was much the same as that of the full-toroidal variator because the half-toroidal variator has the type of trunnion shown in Figure 1. Meanwhile, whereas the full-toroidal variator had three rollers per cavity, surface pressure in contact area was smaller than that of half-toroidal variator, and the ratio between the disc radius and the roller curvature radius became small in comparison with that of the half-toroidal variator.

Figure 9 shows calculated results. Maximum temperature rise was 42 K in the traction contact area on the input disc side of half-toroidal variator. Maximum temperature rise reached 294 K in the full-toroidal variator, and reached 414 °C when considering a bulk temperature of 120 °C. Temperature values in the traction contact surface in Figure 10 were calculated without considering the measured temperature that was two times higher as shown in section 3.2. Thus actual temperature rises are expected to be even higher.

Table 2 Calculated conditions of the temperature rise in the traction contact surface of toroidal CVTs (i_v = -2.236; Calculated conditions for figure 9)

	Half toroidal	Full toroidal
Cavity Diameter, D (mm)	132	110
Disc radius, R_0 (mm)	40	50
Roller radius, R_{22} (mm)	32	30
Radius of rotation to contact point of output disc, r_3 (mm)	69.8	76.0
Half cone angle, θ_0 (deg)	62.5	90
Number of power rollers, n	2	3
Max. Hertz pressure, P (MPa)	3.78	3.19
Spin ratio, ω_{sp}/ω_1	0.09	0.91
Traction coefficient, μ	0.06	
Variator input torque, T_{Vin} (Nm)	350	
Input revolution, N_{in} (rpm)	6 000	
Oil temperature, θ_{oil} (°C)	120	
Bulk temperature, θ_M (°C)	120	

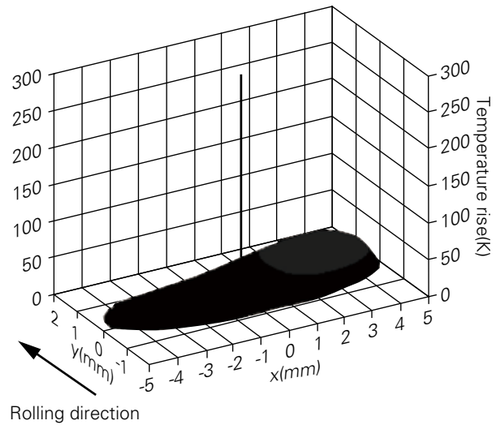

(a) Half toroidal

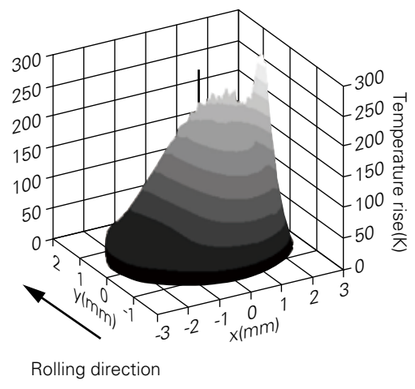

(b) Full toroidal

Fig. 9 Calculated temperature rise on the traction contact surface of the input discs without the correction factor of 2.0 (i_v = –2.236; T_{Vin} = 350 Nm; N_{in} = 6 000 rpm; See table 2)

4.2 Influence of half-cone angle on temperature rise

Next, influence of the half-cone angle on temperature rise was investigated. Specifications of the toroidal CVT used for calculation were the same as the specifications used in reference 12 (research investigating the relationship between half-cone angle and loading devices), and additional specifications of a 53.8 degree half-cone angle θ_0 where a spin ratio of 0 was added. By making equal both the contact point radius of the input disc and the contact point radius of the output disc at maximum speed change, specifications of the toroidal configuration described in Tables 3 and 4 were used.

Figure 11 shows the maximum temperature rise, the maximum Hertz surface pressure, and the absolute value of calculated results of spin ratio in the traction contact area of the toroidal CVT input disc of with the half-cone angle changed. The maximum value of temperature rise became minimum when the half-cone angle θ_0 was

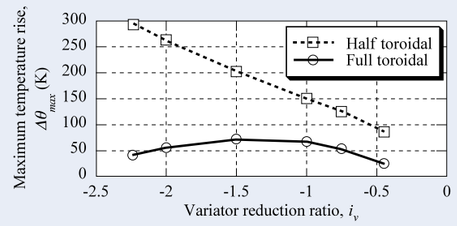

Fig. 10 Calculated maximum temperature rise on the traction contact surface of toroidal CVTs (T_{Vin} = 350 Nm; N_{in} = 6 000 rpm; See table 2)

Table 3 Specifications of toroidal CVTs (i_v = -1.0; Calculated conditions for figures 11 and 12)

Half cone angle, θ_0 (deg)	Cavity diameter, D (mm)	Spin ratio, ω_{sp}/ω_1
50	138.5	-0.15
(53.8)	(135.3)	(0.00)
60	130.0	0.22
70	119.2	0.52
80	107.1	0.78
90	94.4	1.00

Table 4 Common specifications of toroidal CVTs (Calculated conditions for figures 11 and 12)

Disc radius, r_0 (mm)	40
Roller radius, r_{22} (mm)	32
Variator reduction ratio, i_v	-1.0
Traction coefficient, μ	0.06
Variator input torque, T_{Vin} (Nm)	340
Input revolution, N_{in} (rpm)	4 000
Oil temperature, θ_{oil} (°C)	80
Bulk temperature, θ_M (°C)	80

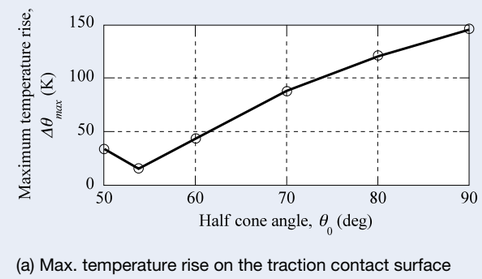

(a) Max. temperature rise on the traction contact surface

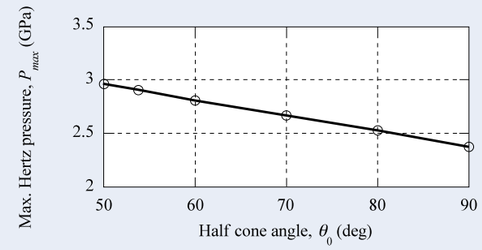

(b) Max. Hertz pressure at the traction contact surface

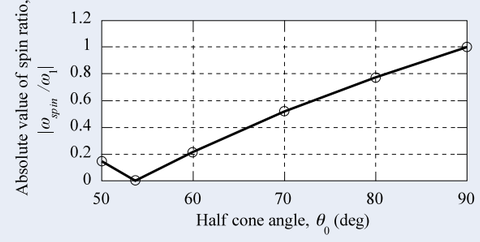

(c) Absolute spin ratio

Fig. 11 Calculated temperature rise on the traction contact surface of toroidal CVTs without the correction factor of 2.0 (i_v = –1.0; T_{Vin} = 340 Nm; N_{in} = 4 000 rpm; See tables 3 and 4)

53.8 degrees. The maximum value of temperature rise increased in proportion to an increase in the half-cone angle and was at the maximum when θ_0 was 90 degrees. Compared with 60 degrees of θ_0 (half-toroidal variator), the maximum value of temperature rise was threefold when θ_0 was 90 degrees (full-toroidal variator). Hertz surface pressure becomes small with an increase in the half-cone angle. Meanwhile, the absolute value of spin ratio was small because the plus/minus spin ratio switches at 53.8 degrees of θ_0 where spin ratio becomes 0 in the area between 50 and 60 degrees of θ_0. With an increase in half-cone angle θ_0, spin ratio also increases as well as the maximum value of temperature rise. Figure 12 shows the calculated traction curve. The slip ratio, with a traction coefficient setting of $\mu = 0.06$, was small at less than 1 %, while the half-cone angle θ_0 was less than 60 degrees in the half-toroidal variator, and became large by more than 2 % at a half-cone angle θ_0 of more than 70 degrees, while reaching 3.6 % at a half-cone angle θ_0 of 90 degrees in the full-toroidal variator.

The traction coefficient was set at a value multiplying the maximum traction coefficient by a given safety factor for the toroidal CVTs. Therefore, slip ratios at the designed traction coefficient largely were defined by the corresponding traction curve. As evidenced in section 3.2, slip ratio highly influences temperature rise. Inclination of the traction curve was large in half-toroidal variator because spin was small, and the slip ratio at the designed traction coefficient became small. As a result, it is considered that heat generation in the contact area is small. Meanwhile, inclination of the traction curve was small in the full-toroidal variator because spin was large, and that the spin ratio became large. As a result, it is considered that heat generation in the contact area was large.

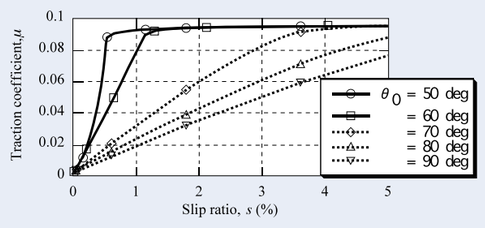

Fig. 12 Calculated traction curve (i_v = –1.0; T_{Vin} = 340 Nm; N_{in} = 4 000 rpm; See tables 3 and 4)

5. Conclusions

Heat generation in the traction contact area with spin motion was investigated in this research, and the following conclusions were obtained:

(1) Comparing measured results of temperature rise in the traction contact area with calculated results using the traction analysis program with the flash temperature theory for verification, it showed that the traction analysis program can simulate the tendency of temperature rise while considering spin/no-spin conditions.

(2) Calculated results of maximum temperature rise in the full-toroidal CVT having large spin reached approximately 300 K. Meanwhile, calculated results of maximum temperature rise in the half-toroidal variator having small spin were approximately 70 K.

(3) With increase in half-cone angle, slip ratio at the designed traction coefficient increased and the maximum value of temperature rise increased proportionally.

Acknowledgments

This research was carried out at the Technical University of Munich when the primary author was a guest researcher while enrolled in doctor's degree program at the Tokyo Institute of Technology, Japan. The authors would like to express their appreciation to Prof. Haruo Houjoh of Tokyo Institute of Technology for his support of this research project.

References

1) Tanaka, H., Toroidal CVT (in Japanese), (2000) Corona publishing Co., Ltd.

2) Hata, K. and Aoyama, S., Traction drive CVT and traction oil for automobiles, Idemitsu Tribology Review (in Japanese), 12 (1986) pp. 702-712

3) Dowson, D., Taylor, C. M. and Xu, H., Elastohydrodynamic lubrication of elliptical contact with spin and rolling, Proc. L. Mech. E., Part C, 205 (1991) pp. 165-174

4) Taniguchi, M., Dowson, D and Taylor, C. M., The effect of spin motion upon elastohydrodynamic elliptical contacts, Proc. of the 23rd Leeds-Lyon Symposium on Tribology, (1997) pp. 599-610

5) Johnson, K. L. and Teverwaark, J. L., Shear behavior of elastohydrodynamic oil films, Proc. Roy. Soc. Lond., Ser. A, 356 (1977) pp. 215-236

6) Graswald, C.: Reibung im elastohydrodynamischen Kontakt von Reibradgetriebe, Diss. TU München (in Germany), (2001)

7) Ishikawa, K. and Tanaka, H., Power transmission of half-toroidal traction-drive CVT - 7th report, Temperature-rise of power-roller-, Proc. of the 73rd JSME Fall Annual Meeting (in Japanese), (1995) pp. 264-265

8) James, I., Lee, A. and Evans, S., Increasing power density in a full toroidal variator, 3rd International IIR Symposium, Innovative Automotive Transmissions, (2004)

9) Yamamoto, K., A study of power roller bearings in a toroidal CVT, J. of Japanese Soc. of Tribologists (in Japanese), 47, 7 (2002) pp. 582-589

10) Miyata, S., Höhn, B.-R., Michaelis, K. and Kreil, O.: Experimental investigation of temperature rise in elliptical EHL contacts, Tribology International, 41, 11 (2008) pp. 1074-1082

11) Crook, A.W., The lubrication of rollers Pt. III - A theoretical discussion of friction and the temperatures in the oil film, Phil. Trans., Series A, 254 (1961) pp. 237-258

12) Imanishi, T., Machida, H. and Tanaka, H., A Geometrical Study of Toroidal CVT, Proc. of 1996 JSAE Annual Congress, 9633207 (1996) pp. 121-124

Shinji Miyata

Bernd-Robert Höhn

Klaus Michaelis

Oliver Kreil

Improvements of Half Toroidal CVT

Hiroki Nishii, Sachiko Noji and Tomohiro Inoue
Future Technology Development Center

ABSTRACT

A Half-toroidal continuous variable transmission (CVT) has been introduced to Japanese automotive market in 1999 and draw an attention for the improvement of fuel consumption, high torque capacity, and excellent ratio change behavior. For further improvement of fuel consumption and torque capacity, development of system like power-split is one of a progress. But it is also important to improve the transmitting efficiency of CVT variator parts such as discs and power rollers as manufacturer of a variator. This paper describes the experimental and calculation results about the new technologies such as improved traction surface profile and crank trunnion and angler contact power roller bearing to achieve higher efficiency and higher torque capacity.

Reprinted with permission from JSAE, CVT-HYBRID 2007 Vol. 20074570

1. Introduction

Main losses of a variator of half toroidal CVT are generated at traction surface and power roller bearings as shown in Fig. 1. The losses of traction surface and power rollers are influenced by their specifications and load. So it is important to optimize specifications and reduce the load for achieving higher efficiency. Loading force for Half toroidal CVT is determined by considering not only necessary load for traction drive but also losses such as swing resistance of power roller and moving resistance of discs and so on. In order to reduce the loading force, it is important to reduce above losses and improve the traction characteristic. This paper describes the measurement and calculation result about the surface profile of traction surface and newly-developed power roller support structure called crank trunnion and the optimum specifications of power roller bearings.

2. Efficiency Test

2.1 Relation between traction coefficient and efficiency

Efficiency test is performed to obtain the relation between traction coefficient and efficiency. Fig. 2 shows the testing box used for the efficiency test. Regarding the testing box, loading force is not applied by loading cam but hydraulic piston. And Table 1 shows the basic variator specifications installed in the testing box. Relation between traction coefficient and efficiency is measured by changing loading pressure. As a result efficiency goes up in proportion to the increase of traction coefficient. Fig. 3 shows the measurement result on condition that input torque is 350 Nm, CVT variator reduction ratio is 1, and input revolution is 2 000 rpm. From the result, it is found that higher traction characteristic or reduction of necessary loading force can improve the efficiency.

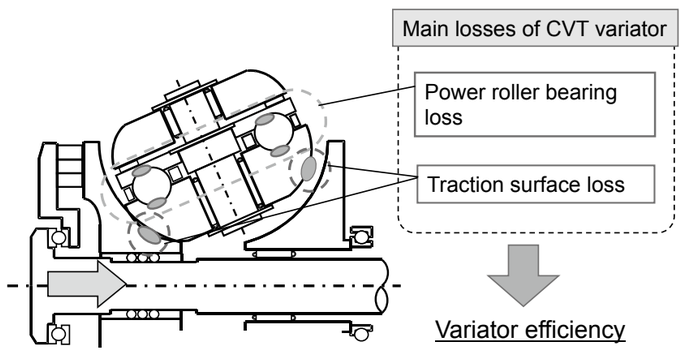

Fig. 1 Main losses of CVT variator

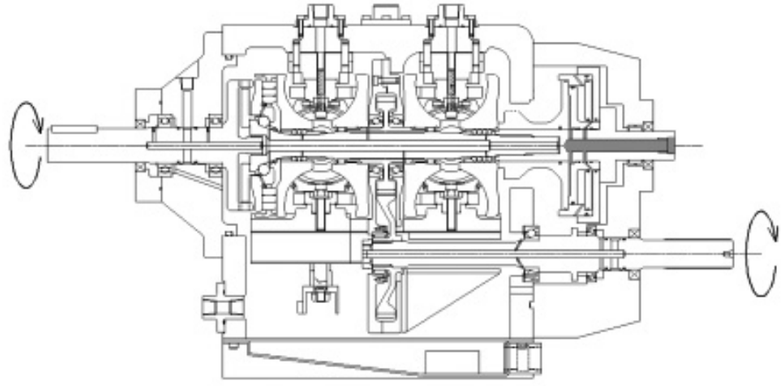

Fig. 2 Testing box

Table 1 Variator basic specifications

Cavity diameter [mm]	132
Disc radius [mm]	40
PR radius [mm]	30
Contact angle [deg]	125

Table 2 Processing method

No.	Groove processing	Radius processing
1 (conventional)	None	None
2	Grind	SF
3	SF	None
4	SF	Fine shot

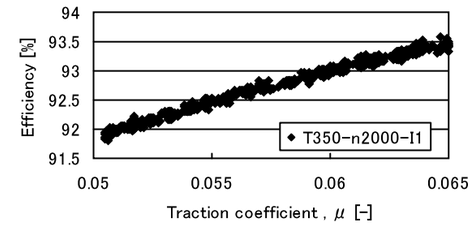

Fig. 3 Relation between traction coefficient and efficiency

3. Improvement of Traction Characteristic

As described in above, improvement of traction characteristic effects improvement of variator efficiency. So it is important to investigate the optimum surface profile of traction surface that transmit the power. The relationship between surface profile of traction surface and traction characteristic is measured and calculated. And the optimum surface profile is also investigated.

3.1 Surface profile of the prototype

Traction surface of input side disc and output side disc are produced with the processing method shown in Table 2 experimentally and tested and calculated. Fig. 4-7 shows the measured surface profile produced by No. 1-4 method.

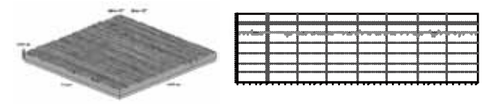

Fig. 4 Surface profile of No. 1

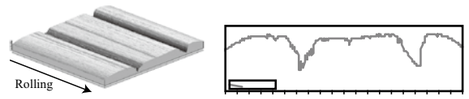

Fig. 5 Surface profile of No. 2

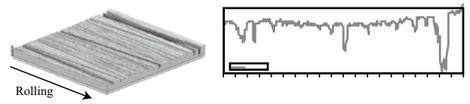

Fig. 6 Surface profile of No. 3

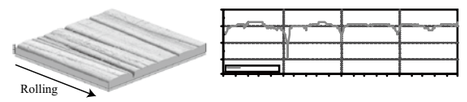

Fig. 7 Surface profile of No. 4

3.2 Measurement

Prototype version of discs whose surface profile is No. 1-4 are produced and used for the measurements of maximum traction coefficient and durability test. The condition of maximum traction coefficient measurement is shown in Table 3, and that of durability test is shown in Table 4. The testing box and the basic variator specifications are same as Fig. 2 and Table 1.

Maximum traction coefficient is measured according to following procedure. First step is setting the condition shown in Table 3 and second is reducing loading pressure and last is calculating traction coefficient when gross slip is happened.

Regarding the procedure of the durability test, first step is setting the condition shown in Table 4 and measuring time when the traction surface is damaged.

3.3 Measurement result

Table 5 shows the result of maximum traction coefficient and durability. Regarding the test condition of maximum traction coefficient, the oil temperature is 85 °C and CVT reduction ratio is 1. And its values are comparison values obtained by setting traction coefficient of No. 1 equal to μ_{st}. Judgments of durability test are determined by the durability time and failure mode.

3.4 Calculation

By using micro EHL analysis program[1], traction coefficient and metal contact ratio are calculated. As same as in the case of the measurement , traction coefficient and metal contact ratio when the oil temperature is 85 °C and CVT reduction ratio is 1 are calculated. In this program viscosity-pressure relation and sheer thinning property are obtained by below mentioned section (1) and (2). And traction coefficient is obtained by section (3).

(1) Viscosity-pressure relation

Viscosity-pressure relation is obtained by using formula (1)[2]. In this regard , however viscosity is set to 10^{12} Pa·s when calculated viscosity is 10^{12} Pa·s or over.

$$\eta_p = \eta_0 \exp[\alpha_0 \cdot p / \{\exp(C_H \cdot p) + (1/A)_0 \cdot \exp(C_J \cdot p) \cdot \alpha_0 \cdot p\}] \quad (1)$$

$$CED = 0.0204\,(t+273)\,(dt/MW)\ln(2.51\,\eta t\,MW)$$

$$(1/A)_0 = a\,(CED) + b$$

$$C_J = c\,(CED) + d$$

$$C_H = e\,(CED) + f$$

(2) Shear thinning property

Slip ratio is high on the measurement condition. So it is necessary to consider sheer thinning property. Sheer thinning property is obtained according to Eyring viscous model adopted in micro EHL analysis program. In formula (2) of Eyring viscous model, τ_0 is set to 5.5 Mpa calculated with the measurement condition. And relationship between $\dot{\gamma}$ and τ is obtained by the formula (2).

Fig. 8 shows the shear thinning property used for the analysis.

$$\frac{1}{\eta^*} = \frac{\dot{\gamma}}{\tau} = \frac{1}{\eta}\frac{\tau_0}{\tau}\sinh\left(\frac{\tau}{\tau_0}\right) \quad (2)$$

(3) Traction coefficient

After performing micro EHL analysis, traction coefficient is obtained by the formula (3). In this formula, traction coefficient of the traction oil is obtained according to Fig. 9. Fig. 9 shows the procedure of calculating traction coefficient of the oil. Pressure peak obtained by micro EHL analysis is evened out and average height of pressure peak is calculated. And average pressure is calculated by multiplying average height of pressure by constant of proportion obtained by the measurement.

$$\mu = f_m\mu_m + (1-f_m)\mu_f \quad (3)$$

f_m : metal contact ratio

μ_m : metal friction coefficient (= 0.1)

μ_f : traction coefficient of traction oil

$\mu_f = \mu_{st}\,(P_{mean} + a\,P_p)/P_{mean}$

P_{mean} : average pressure

P_p : average height of pressure peak

a : constant of proportion

Table 3 Condition of the traction test

Input torque Tin [Nm]	350
Input revolution Nin [rpm]	2 000
Reduction ratio Icvt [-]	0.7 1.0 1.5
Oil temperature Thin [deg]	85 100 120

Table 4 Condition of durability test

Input torque Tin [Nm]	294
Input revolution Nin [rpm]	4 000
Reduction ratio Icvt [-]	1.938
Oil temperature Thin [deg]	110
Traction coefficient μ [-]	0.055

Table 5 Measurement result

No.	max μ ($/\mu_{st}$)	Durability result
1	1.000	OK
2	1.054	NG
3	1.073	NG
4	1.030	OK

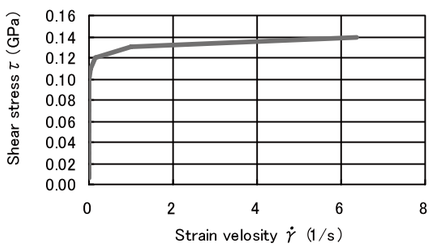

Fig. 8 Shear thinning property

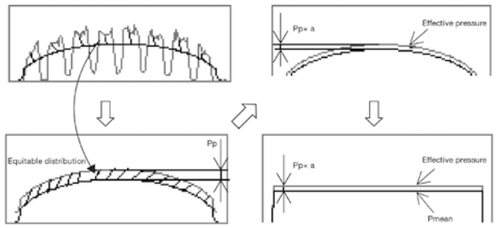

Fig. 9 Procedure of calculation

3.5 Comparison between measurement and calculation

Table 6 shows the comparison between measurement and calculation of No. 1 – No. 4. As a result correlation between measurement and calculation is found in both traction coefficient and durability.

3.6 Optimum surface profile

Optimum surface profile is investigated by using micro EHL analysis program.

(1) Examination surface shape

Fig. 10 shows cross-section shape of surface which is examined. Each parameter shown in Fig. 10 is changed for investigating the optimum shape.

Table 6 Comparison between measurement and calculation

No.	Meaurement		Calculation	
	$\mu_{measure}$	Durability	μ_{cal}	f_m [%]
1	1.000	OK	1.000	0
2	1.054	NG	1.063	7
3	1.073	NG	1.064	10.6
4	1.030	OK	1.021	0

(2) Examination result

Relationship between following parameter and metal contact ratio and traction coefficient is examined. Fig. 11-16 show the examination result. As s result, the shape shown in Table 7 is optimum cross-section shape that can increase traction coefficient without metal contact.

· Pg / Dg
· Rc / Pg
· Wg / Wc

Pg : Groove pitch, Dg : Groove depth
Rc : Convex radius, Wg : groove width
Wc: Convex width

4. Crank Trunnion

Power roller swings on trunnion with eccentric pivot shaft. Reduction of necessary force for swinging motion of power roller makes loading force smaller. Thus crank trunnion that can reduce force of swinging motion and manufacturing cost is newly-developed. Fig. 17 shows the conventional trunnion and Fig. 18 shows the crank trunnion.

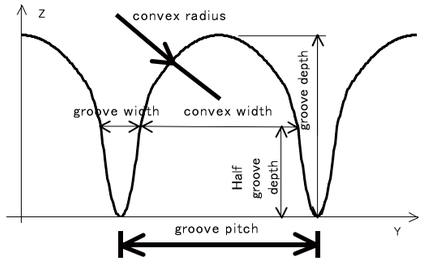

Fig. 10 Examination surface shape

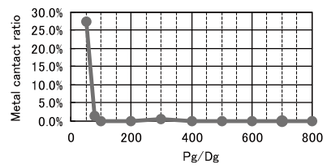

Fig. 11 Pg / Dg – Metal contact ratio

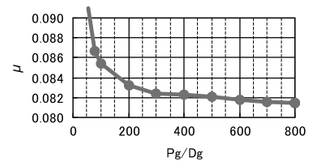

Fig. 12 Pg / Dg – μ

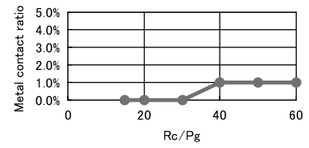

Fig. 13 Rc / Pg – Metal contact ratio

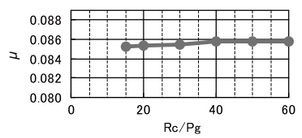

Fig. 14 Rc / Pg –μ

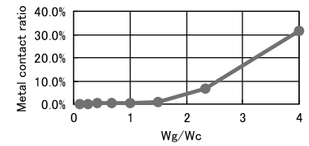

Fig. 15 Wg / Wc – Metal contact ratio

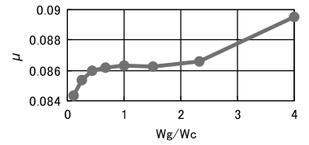

Fig. 16 Wg/Wc-μ

Table 7 Optimum shape

Parameter	Optimum value
Pg / Dg	100 or over
Rc / Pg	30 or less
Wg / Wc	0.25 or less

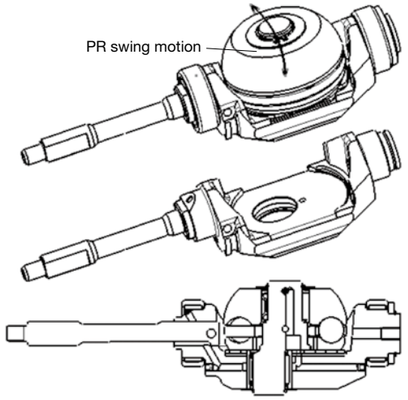

Fig. 17 Conventional trunnion

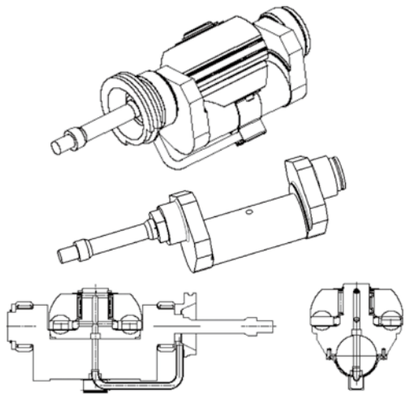

Fig. 18 Crank trunnion

4.1 Calculation of swinging resistance

The swinging resistance of crank trunnion is calculated and compared with that of conventional trunnion. The swinging resistance of crank trunnion is obtained according to Fig. 19 and formula (4) and that of conventional trunnion is obtained by formula (5). Table 8 shows the investigation conditions. And basic variator specifications used for the calculation is same as Table 1.

$$F_s = \mu_m F_{pr} (H1 / H2) + 2\mu_m\mu_t F_c \quad (4)$$

$$F_s = \mu_m F_{pr} + 2\mu_r\mu_t F_c \quad (5)$$

μ_m : metal friction coefficient (= 0.1)

μ_r : rolling resistance (= 0.015)

F_c : contact force

Table 8 Investigation condition

Input torque [Nm]	350
Reduction ratio [-]	0.5 , 0.7 , 1.0 , 1.5 ,1.938
Traction coefficient [-]	0.055

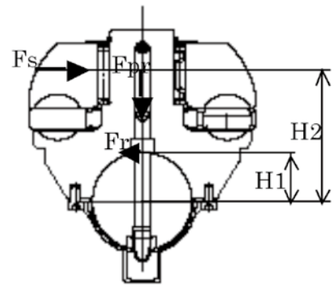

Fig. 19 Crank trunnion

4.2 Calculation result

Fig. 20 shows the calculation result on condition of Table 7. As a result, crank trunnion can reduce 40 % swinging resistance compared with conventional trunnion.

And the loading force can be reduced in proportion to the difference of swinging resistance. Fig. 21 shows the reduction ratio of loading force on each conditions. About 4.5 % loading force reduction is achieved in all CVT reduction ratio.

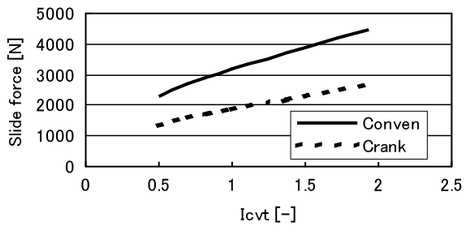

Fig. 20 Slide force

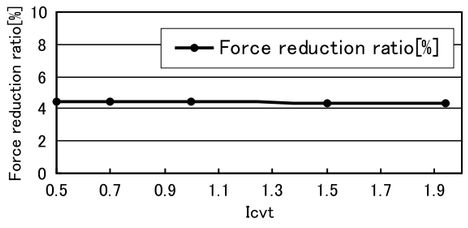

Fig. 21 Force reduction ratio

5. Angular Contact PR Bearing

A contact angle of conventional power roller bearing is 90 deg. Angular contact power roller bearing can reduce the spin but increase the load for each ball. So it used to be considered that efficiency with angular contact is not improved.

Loss of power roller bearing is depending on a deformation of inner ring due to contact force, a deformation of outer ring due to a deformation of trunnion, traction force on radial direction, and so on. Thus the measurement of efficiency with power rollers whose contact angle is 70, 90 and 110 deg is performed. Power rollers integrated with pivot shaft shown in Fig. 22 are used in this measurement. Table 9 shows the measurement condition. And testing box used for the measurement is same as Fig. 2 and Table 1

5.1 Result of the efficiency measurement

Fig. 23 shows the result of efficiency measurement. Efficiency value is indicated by efficiency of the testing box including losses of gear mesh, supporting seals, bearings and so on. As a result, efficiency with 110 deg contact angle power roller is highest, followed by 90 deg, 70 deg. And efficiency of 110 deg is higher than that of 90 deg by 0.2 % in any conditions.

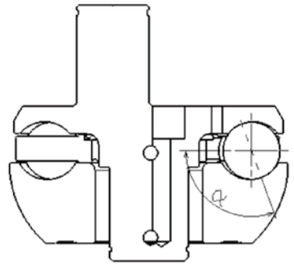

Fig. 22 Integrated powerroller

Table 9 Condition of the efficiency test

PR Brg anguler angle [deg]	70 , 90 , 110
Input torque [Nm]	200 , 250 , 300 , 350
Reduction ratio [-]	0.7 , 1.0 , 1.5
Traction coefficient [-]	0.055

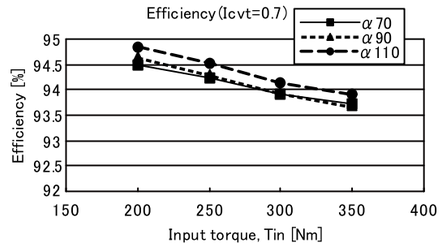

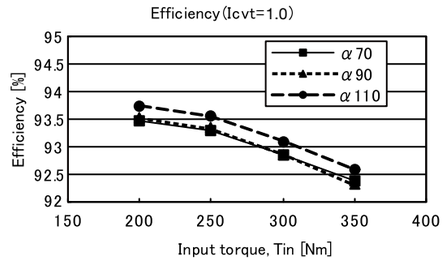

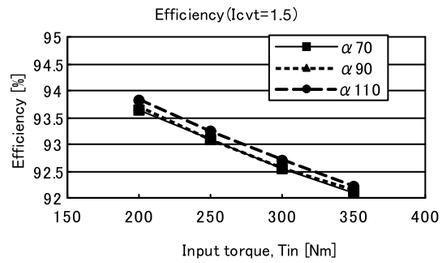

Fig. 23 Measurement result

6. Improvement of Efficiency

Assuming that optimum surface profile increases traction characteristic by 5 %, and crank trunnion reduces loading force by 5 %, necessary loading force is reduced by 10 %. In this case, actual use of traction coefficient is increased by 10 %. In case of 10 % higher traction coefficient, efficiency of testing box is improved by 0.6 % according to the traction coefficient-efficiency relation shown in Fig. 3.

With the efficiency improvement of angular contact power roller efficiency of variator is improved by 0.8 %.

7. Conclusion

Optimum traction surface profile that can balance the improvement of traction characteristic and durability is obtained by measurement and calculation.

Crank trunnion that can reduce loading force compared with conventional trunnion is newly-developed.

Regarding the integrated power roller, efficiency is improved by expanding its contact angle from 90 deg.

With above three effect, the efficiency is improved by 0.8 % and the efficiency of improved variator including integrated power roller and hydraulic loading and three effect is estimated 97 %.

Future tasks are testing the optimum traction surface that is calculated with micro EHL analysis program, theoretical calculation of contact angle-efficiency relation in consideration of deformation, and bringing further improvement to half toroidal CVT.

References

(1) Epstein, D., et al., "Effect of Surface Topography on Contact Fatigue in Mixed Lubrication", Tribology Transactions, Vol. 46 (2003) 4, 506-513

(2) Hata, K., et al., "Various function and property of IDEMITSU traction oil", IDEMITSU Tribo review, No. 28, 2005, p 23-34

(3) Nanbu, T., et al., "The effect of surface roughness on elastohydrodynamic traction (1)", Proc. Int. trib. Conf. Nagasaki (2000) p 637-642

(4) Yamamoto, T., et al., "Calculation Analysis on Efficiency and Fatigue Life Influenced by Deformation of Rolling Elements in a Toroidal CVT", JSAE, Vol. 35, No. 2, April 2004

(5) C R Evans, et al., "The influence of surface roughness on elastohydrodynamic traction", Proc Instn Mech Engrs, 201, No. C2 (1987) pp 145-150

Hiroki Nishii

Sachiko Noji

Tomohiro Inoue

Development of World's Thinnest* Drawn-Cup Needle Roller Bearings with Seal Ring

—The Need for Improved Fuel Economy and the Application of Needle Roller Bearings

Takashi Ono and Hiromichi Takemura
Automotive Bearing Technology Center

ABSTRACT

Sleeve bearings, also called bushings, are used to support rotating shafts, such as those used in an automobile engine and transmission. There are, for example, about ten bushings in an automatic transmission. Drawn-cup needle roller bearings with seal rings support rotating shafts in the same way as bushings do, and work to control the flow of lubricant. Rotating torque (rotational resistance) can be reduced to 50 percent by replacing bushings with drawn-cup needle roller bearings with seal rings. NSK's development of an extremely thin seal ring with a thickness of only 0.85 mm enables the replacement of thin-walled bushings (bushings with a 1.5 mm cross section), which until now was not previously possible. This product helps to improve the fuel economy of newer automobiles.

1. Introduction

At present, between 10 and 15 plain bearings (bushings) are used in automatic transmissions (ATs) for front-engine, rear-wheel drive (FR) automobiles, and between 5 and 10 bushings are used in ATs for front-engine, front-wheel drive (FF) automobiles. Recent ATs are required to meet demands for a smooth ride and high efficiency, and as a result, the operating conditions of bearings have become increasingly severe in line with the needs of the increased number of gear ratios, higher rotational speeds, more compact housings, and higher loading capacity requirements.

Particularly, the needs for greater wear resistance and seizure resistance under greater high-speed rotating conditions for bushings, which are used in large numbers, have been increasing. Meanwhile, bushing makers must accelerate changing bushing materials to lead-free materials, which are more environmentally friendly, and further develop the performance of these bushing expeditiously.

In response to these market demands, there are cases where ATs were retrofitted with drawn-cup needle roller bearings with seal rings. However, one drawback of a conventional drawn-cup needle roller bearing with a seal ring (Figure 1 (a)) is the 3.0 mm to 3.5 mm section height, which is larger than that of a bushing. When the cross-section height is 1.5 mm, a drawn-cup needle roller bearing without a seal ring (Figure 1 (b)) is adopted, which offers superior high-speed rotating performance, but faces the problem of no oil-flow control in the AT. To address this conundrum, NSK developed the world's thinnest drawn-cup needle roller bearing with a seal ring (Figures 1 (c) and 2) whose section height was narrowed by approximately 50 % that of a conventional drawn-cup needle roller bearing with a seal ring, which achieved the same thin profile as that of a bushing.

This article describes the features and offers examples of where the world's thinnest drawn-cup needle roller bearing with a seal ring can be used in ATs.

2. Features of World's Thinnest Drawn-cup Needle Roller Bearing with a Seal Ring

Thin cross-section, drawn-cup needle roller bearings with seal rings have the following features.

(1) Compact

Lowering the bearing cross-section height makes it possible to switch from bushings to needle roller bearings.

Highly precise press forming was applied to produce a metal seal ring with a cross-section thickness of 0.85 mm. This resulted in reducing the bearing's overall cross section by nearly half (Figures 1 (c) and 2) compared to a conventional drawn-cup needle roller bearing with a seal ring (cross-section height: 3 mm to 3.5 mm) to 1.5 mm.

(2) Improved wear resistance and seizure resistance

Even under conditions of decreasing oil supply to the bearing portion, rolling bearings are able to retain smooth rotation in comparison with that of bushings (Figure 4). Under conditions of high-speed rotation and lack of lubricant, wear on a scale of 100 µm occurs in some cases when bushings are used.

*According to NSK research as of July 21, 2006

(a) Conventional drawn-cup needle roller bearing with seal ring

(b) Conventional thin cross-section, drawn-cup needle roller bearing without seal ring

(c) Newly developed, thin cross-section, drawn-cup needle roller bearing with seal ring

Fig. 1 Drawn-cup needle roller bearings

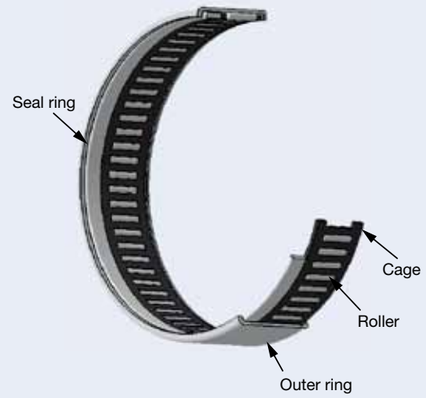

Fig. 2 Cutaway view of the newly developed, thin cross-section, drawn-cup needle roller bearing with seal ring [1)]

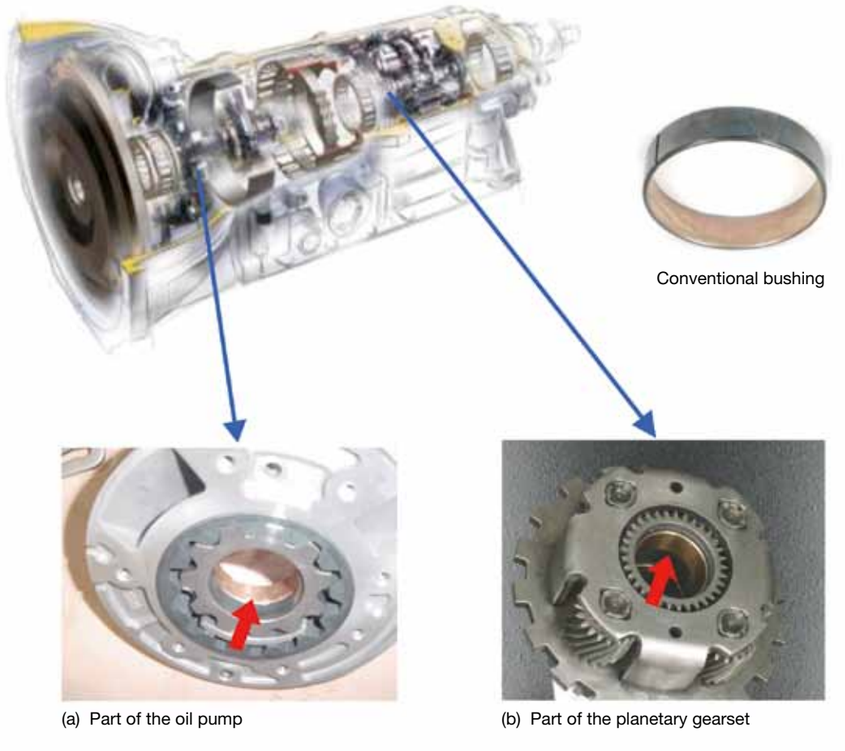

(a) Part of the oil pump

(b) Part of the planetary gearset

Fig. 3 Examples of usage in an automatic transmission

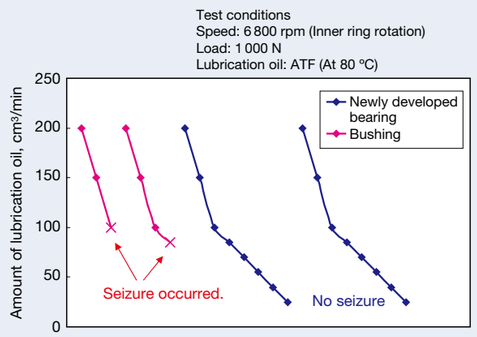

Fig. 4 Comparison of seizure resistance test results [1)]

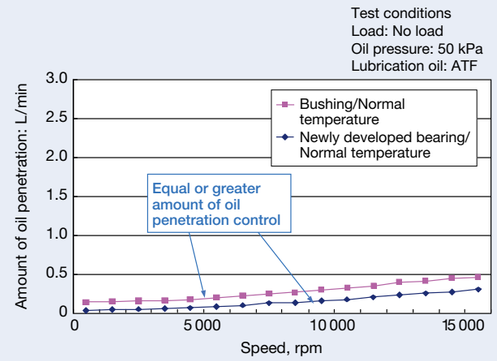

Fig. 6 Comparison of amount of oil penetration

(3) Reduced torque loss with rolling bearings

At the rotational speed (low-speed area between 1 000 rpm and 3 000 rpm), which is more realistic and commonly found in ATs, torque is reduced by approximately 50 % to 95 % in comparison with that of bushings, and energy losses are prevented (Figure 5). If all bushings in an AT are replaced with rolling bearings, fuel consumption can be lowered by 1 % to 2 %.

(4) Control of lubricant flow

The amount and flow of lubricating oil used in ATs that are retrofitted with this bearing are on a par with those of bushings, which results from use of the newly developed, highly precise, thin seal ring (Figures 6 and 7).

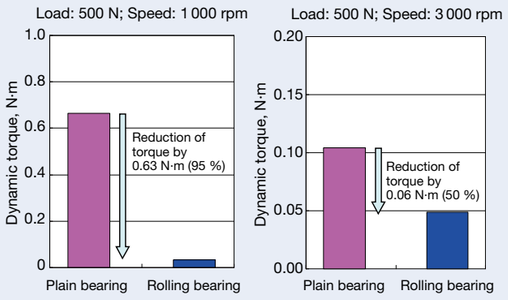

Fig. 5 Comparison of dynamic torque test results

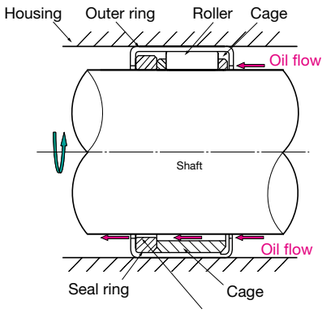

Amount of oil controlled by the clearance between seal ring and shaft

Fig. 7 Features of the thin cross-section, drawn-cup needle roller bearing with seal ring [1)]

3. Application Examples

3.1 Oil pumps

Components within the AT, such as the clutches and brakes, are controlled by hydraulic pressure. The drawn-cup needle roller bearing, and oil pumps, which are used to generate hydraulic pressure, are introduced here.

(1) Oil pump functions [2)]

Automatic transmission fluid (ATF) is recirculated throughout an AT unit, and is the operating oil that is used to apply the clutches and brakes, which are used for changing automobile speed, and is used in the lock-up clutch for applying the torque converter. In addition to these controls, ATF retains internal pressure in the torque converter, lubricates rotating components to prevent seizure, and removes heat from components within the AT, such as clutches, brakes, and torque converters.

The oil pump is required to recirculate ATF within the AT. Pressure that the oil pump supplies to the ATF is called discharge pressure, and the amount that is supplied to the AT is called the discharge rate.

Oil pumps for ATs must maintain a discharge rate with little variance. In other words, only a small amount of fluid can be allowed to leak from the pump even if the fluid is under high pressure. Furthermore, the amount of friction must be minimal, the pulsation of discharge pressure and rate must remain small, operation must remain quiet, and all the applicable components must be compact and lightweight.

(2) AT oil pumps

Gear pumps consist of eccentrically mounted inner and outer rotors, which have a simple structure that facilitates downscaling; and thus, are often used as AT pumps (Figure 3 (a)).

As previously described, the amount of oil that is leaked from the pump must be small in regard to oil-pump functionality. Lower friction can be achieved by switching from bushings to conventional drawn-cup needle roller bearings, but this tends to result in an increased amount of leakage compared to bushings.

With the use of thin drawn-cup needle roller bearings with seal rings, friction can be reduced and the amount of penetrated oil can be controlled, making it possible to retrofit the pump with rolling bearings of the same height as that of a bushing.

3.2 Transmissions

Main components of ATs include a shaft, clutches, brakes, and planetary gears.

Whereas each rotational speed of these components differs at each stage of shifting gears, a mutual rotation occurs. Therefore, bearings (rolling bearings and bushings) are used to support these components. Bearings that operate under loaded conditions in an axial direction tend to be thrust needle roller bearings and those that are loaded in a radial direction tend to be bushings, which both operate at a high-speed rotation (Figure 3 (b)).

Such bushings suffer from a larger amount of torque loss compared with rolling bearings (Figure 5). For the purpose of simply reducing torque loss, it is conceivable to replace bushings with conventional thin drawn-cup needle roller bearings without seal rings. However, the amount of leaked ATF increases compared with bushings as described above, and so the balance of a proper amount of lubrication oil flow to AT components is lost.

Using thin drawn-cup needle roller bearing with a seal ring allows for a bearing with a thinner cross-sectional height and offers the ability to control the amount of penetrated oil. Consequently, replacing bushings with rolling bearings is put into practical use. In addition, it becomes possible to further prevent seizure at high-speed rotation even if the amount of lubrication oil is less than 50 cm³/min.

4. Conclusion

Automobiles will continue to operate with even better fuel economy. Thus, the demand for drawn-cup needle roller bearings with seal rings will continue to increase in the foreseeable future.

We will continue to contribute to a cleaner environment with new product development by meeting market needs as the demand for replacing plain bearings with rolling bearings will expand in hybrid cars and other industries besides automobiles in addition to use in ATs.

This article is a revised version that was published in the monthly publication “THE TRIBOLOGY” (in Japanese).

References

1) NSK Technical Journal Motion & Control, No. 21 (2009) 53-54.
2) Y. Morimoto, “Transmission of AT and Introduction of Control”, (2006) 93-94, Grand Prix Book Publishing (in Japanese).
3) T. Ono and H. Takemura, “The Need for Improved Fuel Economy and the Application of Needle Roller Bearings”, THE TRIBOLOGY, No. 242 (2007. 10) 47-49, Shinjusha Co. Ltd. (in Japanese).

Takashi Ono

Hiromichi Takemura

Technological Trends in Linear Motion Rolling Guides for Machine Tools

Shigeharu Kobayashi
Linear Technology Center

ABSTRACT

As machine tools continue to evolve, various technological demands are being placed on linear motion rolling guides for use in machine tools. Numerous linear guides, which are a type of linear motion rolling guide with a rail, are utilized in machine tools functioning as linear motion components. Using the key concepts of high capacity, high rigidity, and high precision, in addition to improving the working environment, this article introduces various issues that face linear guides and the measures required to resolve them.

1. Introduction

Although the speed of machine tools has become remarkably faster in recent years, greater emphasis is being placed on reducing overall processing time and shortening cycle times (takt time) of complex, multifunctional machine tools. Thus, the conditions under which linear motion rolling guides operate including increased loads due to higher operating speeds and more rapid acceleration and deceleration have led to increased demand for higher load-carrying capacity and a higher degree of rigidity. Furthermore, linear motion rolling guides must meet stringent requirements for high quality workmanship and high accuracy for processing of more complex fine shapes. Specifically, there are great expectations from the fields of machinery and electronic equipment, micro-optics, and the medical field. In addition, extending replenishment intervals of lubricant and maintenance-free performance are strongly expected.

A variety of linear guides from among various linear motion rolling guides are being used as guides in machine tools. As applications using linear guides expand, various technological developments that respond to future requirements for linear guides are being carried out.

This article introduces issues and efforts that have been taken to address the demands being placed on linear guides with a focus on key concepts of high loading capacity and high rigidity, high precision, and environmental issues.

2. High Loading Capacity and High Rigidity

In recent years, there has been a trend towards increasingly complex and multispindle machine tools, which are capable of intensive processing. Furthermore, demand has grown for shorter machining cycles and shorter takt times. Consequently, loads being placed on linear guides have increased under operating conditions of higher speeds, and more rapid acceleration and deceleration cycles resulting in increased demand for linear guides with greater rigidity that meet requirements for higher precision. Lately, the adoption of machine tools using highly rigid roller guides with high load-carrying capacity is progressing, especially in Europe.

The basic dynamic load rating for roller guides is defined in International standards ISO 14728-1:2004:

$$C_{100R} = bm \cdot f_c \cdot l_t^{1/36} \cdot i^{7/9} \cdot Z_t^{3/4} \cdot L_{WE}^{7/9} \cdot D_{WE}^{35/27} \cdot \cos\alpha$$

where $f_c = \lambda \cdot 195$, $bm = 1.1$, $\lambda = 0.83$

C_{100R}: Basic dynamic load rating rated at 100 km
λ: Reduction coefficient
l_t: Effective slide length
i: Number of raceways
Z_t: Number of effective rolling elements
L_{WE}: Effective roller length
D_{WE}: Roller diameter
α: Contact angle

According to this formula, the diameter of a roller (rolling element) has the greatest impact on load rating. This is equally true when balls are used as the rolling elements in a linear guide.

If excessive contact pressure (edge loading) occurs at the roller end, roller guide life is generally reduced. Therefore, ends of the rollers are designed with a beveled portion called crowning to prevent edge loading. However, excessive crowning can reduce the contact area, which becomes a factor that leads to a reduction in loading capacity and rigidity. Thus, FEM analysis is used to design a crowning configuration that achieves an almost even surface pressure distribution over the entire effective length of the roller.

Next, rigidity of the contact area between the rollers and the raceway is much higher than that between balls and a raceway. Furthermore, rigidity of the contact area is relatively higher than that of the component parts, and so the rigidity of the entire roller guide is highly affected by the component parts. As a result, rigidity is calculated and surface pressure distribution is analyzed based on deformation analysis of component parts using an FEM model. Figure 1 shows the relation between external load and deformation for measured and calculated results. Calculations were conducted for a case in which component parts were assumed to be rigid, and for a second case in which rigidity of the materials was incorporated. For the first case, deformation is considerably less than the experimental results, and rigidity is overvalued. Accordingly, this confirms that rigidity of component parts greatly impacts rigidity of the roller guide[1]. In addition, verifications were made where rigidity in the tensile direction changes between 6 % and 25 % by changing the number of mounting bolts on the slider from the conventional four bolts to six bolts. The effect of component-part rigidity is confirmed as a result.

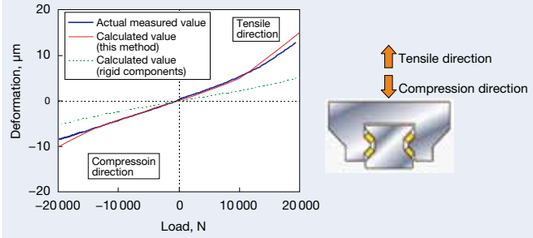

Fig.1 Comparison of calculated and experimental results of roller guide deformation (model size #35)[1]

3. High Precision

Demands for higher grades of finished surfaces have become increasingly severe for die processing machines and precision lathes. Rolling guides that have low friction and are superior in NC-following capability are suitable for use in higher precision machines due to improved NC control. However, errors in linear guide motion accuracy have been a problem in the field of super precision processing, and so hydrostatic guides have been used. However, hydrostatic guides are expensive and lack sufficient vibration damping capability resulting in a growing desire for linear guides with motion accuracy on a par with hydrostatic guides while taking advantage of the use of linear guides, which offer easier handling and relatively lower prices.

Factors affecting diminished motion accuracy of linear guides include vibration induced by rolling element passage, which occurs due to a cyclic variation of the number of rolling elements (as shown in Figure 2), and variations of rail mounting hole pitch caused by tightening the mounting bolts on the slider.

Vibration induced by rolling element passage cannot be avoided due to the structure of the rolling guide. This cycle of passage vibration is approximately twice the diameter of the rolling elements. In addition, the vibration is amplified in proportion to the distance from the linear guide and the cutting (processing) point of the machine tool. Crowning at each end of the raceway of the slide can help reduce such vibration, in addition to applying a method for discovering an optimal shape of crowning to further reduce vibrations[2].

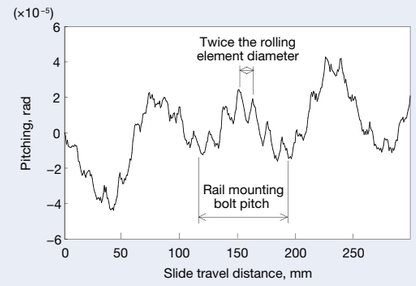

Fig. 2 Motion accuracy test results of an NSK linear guide[3]

Recently, obtaining the magnitude of vibration became a simple process, which made it easier to estimate the magnitude of vibration beforehand based on linear guide specifications. It has been understood that what most affects this magnitude of vibration is the number of effective rolling elements in the loaded zone, that is, slider length and crowning of the raceway[3]. Figure 3 shows the effect of effective number of rolling elements and crowning.

Meanwhile, the issue of rail deflection in a linear guide, which is caused by bolt tightening when fixing the rail to the base component, has been addressed by increasing the counterbore depth of the rail-mounting hole and by reducing the length of the mounting hole pitch. Figure 4 shows the mode of rail deflection caused by mounting bolts. Figure 5 shows the analysis results of the relation

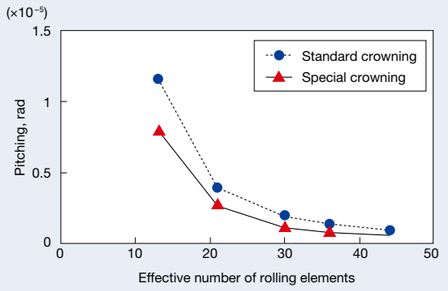

Fig. 3 Effective number of rolling elements and the calculated vibration induced by rolling element passage[3]

between the position of a rail in a longitudinal direction (distance from bolt center) and the amount of deflection at the center position of a lower rail groove.

Motion accuracy of linear guides with super-long specifications where the length of the slider is approximately twice that of a standard slider also been further improved through the application of such analyses. The motion accuracy test results shown in Figure 6 are results of motion accuracy measurements taken with 500 mm of overhang on a table with 8 sliders using standard specifications, or with 4 sliders using super-long specifications. Error of motion accuracy is restricted to less than half in sliders with super-long specifications. Super-long specifications of linear guide have already been adopted for use with super precision tables for precision lathes and die processing machines, and are expected to approach increasingly close to the domain of hydrostatic guides in the future.

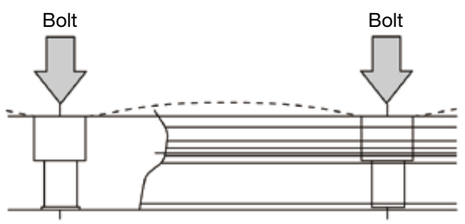

Fig. 4 Mode of rail deformation caused by tightening bolts [3]

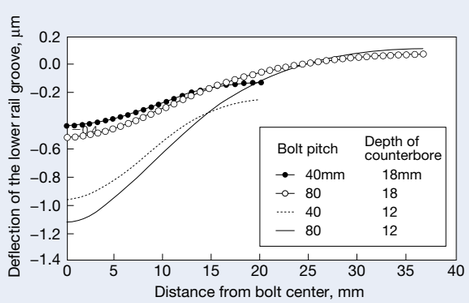

Fig. 5 FEM analysis results of rail deflection due to bolt tightening [3]

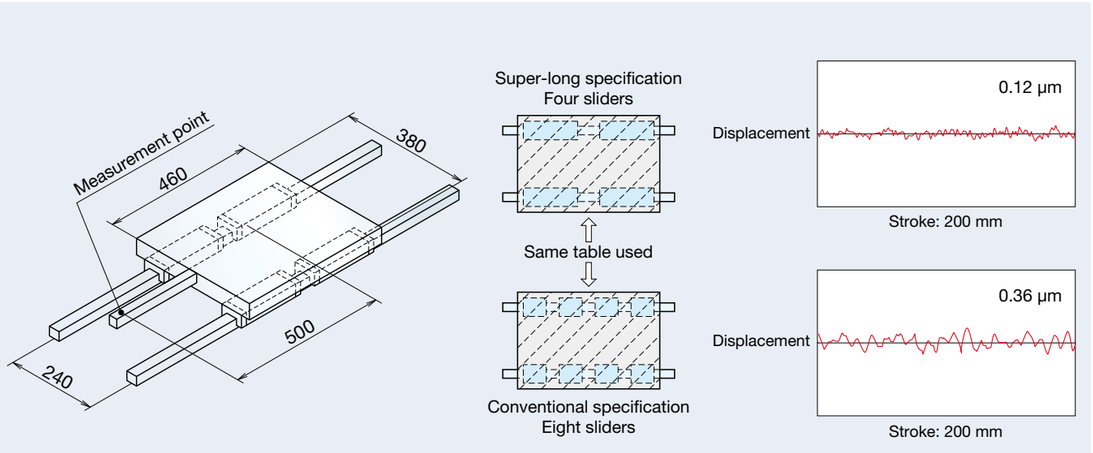

Fig. 6 Motion accuracy test results [4]

4. Environmental Issues

In most applications, grease is the standard lubricant used with linear guides. However, since grease requires frequent and periodical replenishment, extended lubrication intervals and extended maintenance-free performance are in high demand. This problem has been addressed with a so-called “lubrication unit” that mounts onto the slider end face where oil is fed from the unit’s resin material, which allows for a steady supply of lubricant over the long term. This lubrication unit functions over the long-term, providing maintenance-free performance, and helps to extend the service life of industrial machinery and woodworking machinery that would normally consume large amounts of lubricant. Furthermore, the lubrication unit addresses environmental issues associated with old grease, and foul odors associated with lubricating oil becoming mixed with coolants as is the case with machine tools using grease lubrication.

Assuming the operating conditions of a machine tool, severe durability testing was carried out for linear guides being operating under conditions of exposure to foreign matter. Photo 1 shows test conditions, Table 1 lists the test conditions of lubricant and seal, and Table 2 lists the test results.

Photo 1 Linear guide undergoing durability testing [5]

Table 1 Durability test conditions

Contaminated fluid:	Cutting fluid + Cast metal powder (Fluid inside: 2 day / week)
Size of linear guide:	Size of rail width #45
Preload:	Heavy load
External load:	100 N / slider
Feed speed:	Average 24 m/min.
Stroke:	400 mm
Specifications of lubrication and seal	
No. 1:	Grease (initial only) + 4 lubrication units at one side + standard seal
No. 2:	Grease (initial only) + standard double seal
No. 3:	#68 oil (intermittent lubrication) + standard double seal

For grease-only lubricating conditions, contaminated fluids washed the grease away, and running life was cut short to 1/5 that of oil lubricating conditions. However, when using the lubrication unit, wear generation was greatly restricted and a longer running distance exceeding that of oil lubricating conditions was achieved. Based on these results, the lubrication unit has proven to be an effective measure for use with machine tools[5].

In addition, measures to prevent foreign matter from directly adhering to the linear guide have been taken by covering linear guides with a physical barrier such as a bellow for operating environments where a large amount of foreign matter may fall directly onto the linear guide. However, when fine foreign matter or a large amount of foreign matter falls onto the guide, it becomes too difficult to prevent foreign matter from entering the linear guide through the use of such barriers like a bellow. In addition, there are cases where a bellow or similar barrier is impractical due to the structure of equipment. Linear guides that are capable of operating under such conditions have been in high demand. At present, seals with a special multistage lip structure that can be directly mounted to a linear guide have been developed. This seal has a structure where foreign matter is unable to ingress; and lubricant in the slider is blocked from outflow.

Photo 2 shows linear guides with highly dust-proof seals,

Table 2 Durability test results

Sample	Lubrication conditions	Running distance (km)	Continuous run	Clearance (µm)	Flaking
No. 1	Grease + lubrication unit	3 600	Approved	Preload remained	None
No. 2	Grease only (prelubricated at initial stage only)	600	Disapproved	30-40	None
No. 3	Intermittent lubrication	3 000	Approved	15-20	Flaked

Photo 2 V1 series of NSK linear guide [6]

Photo 3 shows the conditions of highly dust-proof seal testing against foreign matter, and Figure 7 shows the results. These results confirm that highly dust-proof seals are effective in reducing the entry of foreign matter by more than 9/10 that of a conventional seal. Under severe test conditions with exposure to foreign matter, service life was fourfold longer when using the lubrication units compared with conventional seals alone.

In addition, synthetic coolants have been used to improve cutting performance in many cases in recent years, which have a detrimental effect on seal materials. Materials superior in coolant resistance or materials made from different compounds are selected for use in linear guides. The effectiveness of such seals has been confirmed through immersion testing in various types of coolant.

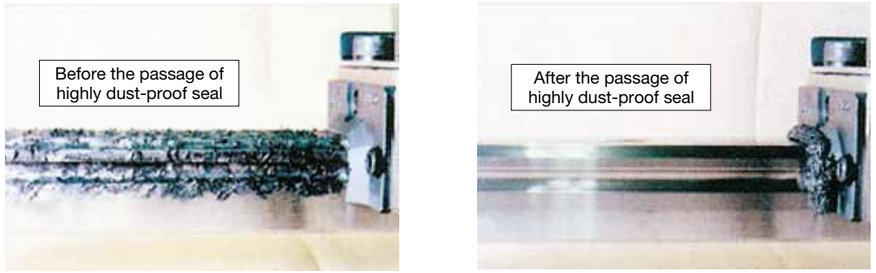

Photo 3 Highly dust-proof seal testing against foreign matter [6)]

5. Conclusion

This article has introduced examples of technological developments related to linear guides in response to demand for higher precision, higher loading capacity, and higher rigidity, and in response to environmental issues pertaining to machine tools. Demands from the machine tool market are anticipated to become increasingly severe in the future and the issues faced by linear guides will continue to change. Further progress in development and analysis will be necessary in order to respond to such changes and the speed of those changes.

It is my hope that this article will contribute to improving the performance of machine tools using linear guides.

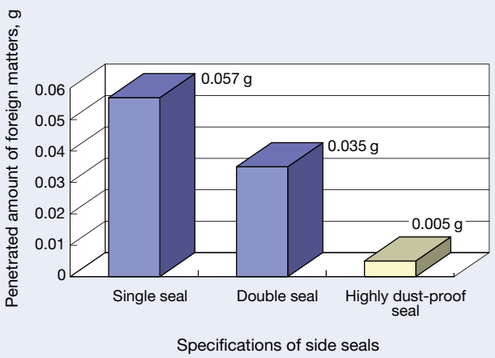

Fig. 7 Results of highly dust-proof seal testing against foreign matter

This article is a revised version that was published in the monthly publication “THE TRIBOLOGY” (in Japanese).

References

1) J. Matsumoto, “Numerical Analysis Technology on NSK Linear Guides for Machine Tools”, NSK Technical Journal, 676 (2003).
2) T. Yamaguchi, “Influence of Ball Screws and Slide Ways on Positioning Accuracy”, NSK Technical Journal, 650 (1989).
3) S. Kato and J. Matsumoto, “Recent Developments in Highly Precise NSK Linear Guides”, NSK Technical Journal, 669 (2000).
4) “High Accuracy Series of NSK Linear Guides”, NSK Catalog, CAT No. 3329 2005 E-9.
5) S. Kato, “Development of NSK K1 Seal for Linear Guides”, NSK Technical Journal, 664 (1997).
6) “V1 Series of Highly Dust-Proof NSK Linear Guide”, NSK Catalog, CAT No. 3330b 2006 E-3.
7) S. Kobayashi, “Technological Trends in Linear Motion Rolling Guides for Machine Tools”, THE TRIBOLOGY, January (2008), 12-15.

Shigeharu Kobayashi

Thrust Needle Roller Bearings with Retention Tabs

In general, most transmissions are vertically positioned to facilitate ease of assembly. In such cases, although a number of thrust needle roller bearings are joined with upper components using petroleum jelly during mounting of the assembly, the thrust needle roller bearings are at risk of being improperly mounted.

To ensure that the bearings are mounted securely, NSK has developed a thrust needle roller bearing with retention tabs.

1. Structure

Retention tabs are incorporated into the bearing race, and can be formed in multiple positions on either the bore diameter or outside diameter sides of the thrust needle roller bearing race.

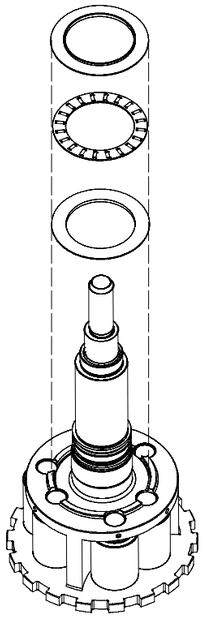

Fig. 1 Exploded view of bearing in a transmission assembly

Photo 1 Newly developed thrust needle roller bearing with retention tabs (tabs on bore diameter side)

Photo 2 Newly developed thrust needle roller bearing with retention tabs (tabs on outside diameter side)

2. Features

Conventional tabs, which have been used to prevent the bearings from being mounted backwards, require heavy loads for mounting, and are susceptible to breaking.

By adopting retention tabs of this shape, the amount of the deformation of tabs can be adjusted to prevent breakage of the tabs during mounting.

Photo 3 Conventional tab

Photo 4 Newly developed retention tab (tab on bore diameter side)

Photo 5 Newly developed retention tab (tab on outside diameter side)

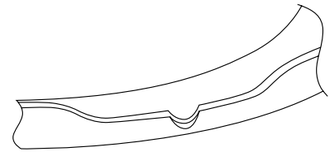

Fig. 2 Close-up drawing of a conventional tab

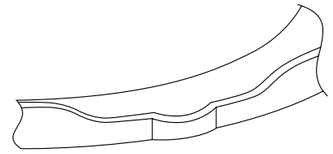

Fig. 3 Close-up drawing of the retention tab

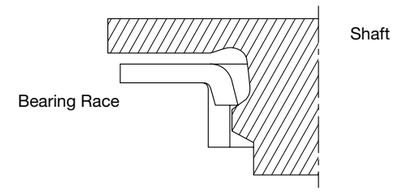

Fig. 4 Example of bearing mounted on a shaft

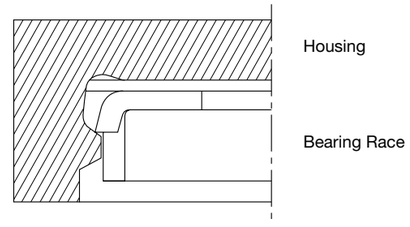

Fig. 5 Example of bearing mounted in a housing

3. Applications

This bearing can be used in automotive transmissions and other components where thrust needle roller bearings are at risk of dropping out during or after mounting. Currently, this series of bearing is being used to ensure secure mounting in the housing or on the shaft of dual-clutch transmissions (DCTs) and automatic transmissions (ATs).

Cartridge-Type Ball Bearings for Turbochargers

The rate at which automotive engines are equipped with turbochargers has been increasing as a means of reducing CO_2 emissions or improving fuel economy. Each car manufacturer is promoting new developments with the aim of both reducing mechanical losses of bearings and improving turbocharger efficiency. This is being achieved by switching from conventional plain bearings, which has been mainstream for turbochargers, to rolling bearings.

NSK has developed a cartridge-type ball bearing for turbochargers that combines the bearing and surrounding components into a single, unitized design for responding to market needs.

Photo 1 Cartridge-type ball bearings for turbochargers

1. Structure

Figure 1 shows the structures of a turbocharger. Figure 1 (a) is an example that includes a cartridge-type ball bearing, and Figure 1 (b) is an example that includes a set of single-row angular contact ball bearings. In both cases, counterbored angular contact ball bearings with one-piece machined cages for high-speed rotation are used.

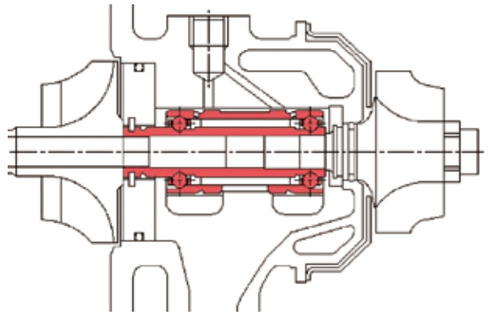

(a) Cartridge-type ball bearing for turbochargers

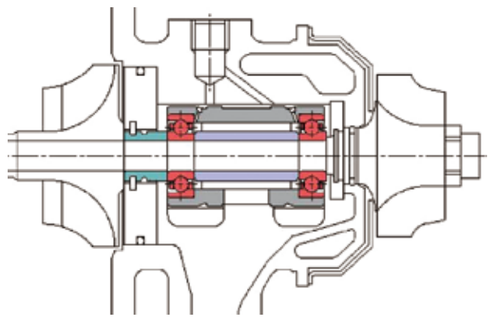

(b) Single-row angular contact ball bearings for turbochargers

Fig. 1 Turbochargers

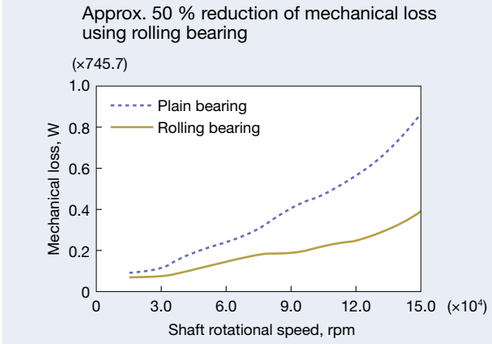

Fig. 2 Comparison of mechanical loss

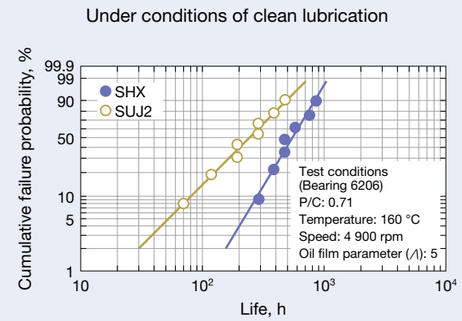

Fig. 3 Life test results of bearings using SHX material under high-temperature conditions

2. Features

Figure 2 illustrates a comparison of mechanical loss of a turbocharger using rolling bearings and a turbocharger using conventional plain bearings. Rolling bearings are able to achieve an approximate 50 % reduction in mechanical loss compared with that of a plain bearing. Features of rolling bearings are described below.

2.1 Improved component accuracy by unitizing the cartridge

Cartridge-type ball bearings improve component accuracy as a unit because the number of components surrounding the bearing such as a sleeve or a spacer can be eliminated. As a result, the imbalances in turbochargers are more accurately corrected. In addition, this bearing leads to shorter assembly time on turbocharger production lines.

2.2 Long life under high temperature conditions

By adopting NSK's newly developed, heat-resistant SHX material for bearing rings, rolling life, heat-seizure resistance, and wear resistance have been improved. Figure 3 shows the life test results of this type of bearing using SHX material under high-temperature conditions.

3. Applications

This unit has already been adopted for use in automotive turbochargers, and is capable of responding to the needs of higher operating temperatures and higher speeds associated with the downsizing of turbochargers.

4. Summary

NSK has sorted out the production system and is mass-producing cartridge-type ball bearings for turbochargers. NSK will continue to develop high performance bearings that respond to market needs.

High-Performance Standard NSKHPS Angular Contact Ball Bearings for Industrial Machinery

The pumps, compressors, gearboxes, and robots that are a part of many industrial machinery must be easy to maintain, have low operating costs, be highly efficient, reduce power consumption, and be environmentally friendly as well as be highly reliable. For this reason, long life, high speed, and high accuracy are demanded of bearings used in such industrial machinery. NSK has developed and commercialized the high-performance, standard NSKHPS Angular Contact Ball Bearings (Photo 1) to meet the needs of industrial machinery.

1. Product Features

Features of the high-performance, standard NSKHPS Angular Contact Ball Bearing for industrial machinery (Photo 1) are as follows:

(1) Longer life

Bearing life has been extended by a maximum of 90 % in comparison with that of conventional NSK products by means of an optimized bearing internal design and the application of NSK's material technology. Together, these efforts have resulted in a bearing that ensures long-term, maintenance-free performance and reduces machinery-operating costs. If equivalent life is sufficient for a given application, the NSKHPS Angular Contact Ball Bearing provides an opportunity to downsize while offering the same power density for the purposes of downscaling and improving energy efficiency of industrial machinery.

(2) Improved limiting speed

Bearing limiting speed has been improved from 15 % to 20 %, compared to the conventional product, through optimal bearing internal design, and precision processing and manufacturing technologies. The higher bearing limiting speed facilitates faster processing by industrial machinery, which contributes to improved work efficiency.

Photo 1 High-performance standard NSKHPS Angular Contact Ball Bearings

(3) Trouble-free and highly precise positioning in axial direction

The precision processing and manufacturing technologies applied to manufacturing this bearing allow for universal arrangement of angular contact ball bearings (Figure 1) of ISO tolerance class P5 running accuracy and ISO tolerance class P6 dimensional accuracy. As a result, this bearing facilitates easier, highly precise positioning (Tables 1 and 2).

Therefore, the NSKHPS Angular Contact Ball Bearing contributes to higher efficiency of machinery in addition to providing ease of assembly and maintenance of industrial machinery.

(4) Availability of three cage types

NSK offers three types (Figure 2) of cage materials to choose from including Nylon 46, which offers high strength under high-temperature conditions; L-PPS resin, which offers superior resistance to oil and chemicals; and brass, which offers a greater degree of reliability. Choosing the appropriate cage material for a given application can greatly contribute to improving the reliability that is required of various industrial machinery.

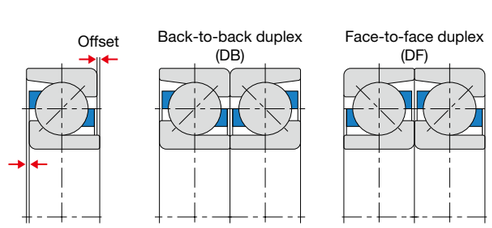

Fig. 1 Examples of bearing arrangements

Table 1 Comparison of bearing accuracy

Example: 7313B (ϕ65 mm × ϕ140 mm) Unit: mm

		Standard bearing	NSKHPS
Dimensional accuracy	Inner ring bore diameter	0/–0.015	0/–0.012
	Outer ring outside diameter	0/–0.018	0/–0.015
Running accuracy	Inner ring radial runout	max. 0.020	max. 0.005
	Outer ring radial runout	max. 0.040	max. 0.011
	Inner ring axial runout	N/A	max. 0.008
	Outer ring axial runout	N/A	max. 0.013
	Inner ring face runout with bore	N/A	max. 0.008
Axial clearance tolerance of combined bearings		0.040	0.012

Table 2 Measured axial clearances

Bore diameter (mm)		NSKHPS CNB (μm)			NSKHPS GA (μm)		
Over	Or less	Minimum	Maximum	Deviation of tolerance	Minimum	Maximum	Deviation of tolerance
12	18	17	25	8	–2	6	8
18	30	20	28	8			
30	50	24	32	8			
50	80	29	41	12	–3	9	12

2. Specifications

NSK offers a lineup of these bearings with bore diameters ranging from 12 mm to 80 mm (Table 3).

3. Summary

High-performance standard NSKHPS Angular Contact Ball Bearings for industrial machinery contribute to lower operating costs by extending maintenance intervals, contribute to downscaling of equipment and reducing energy consumption, improve assembly work efficiency, and improve machine efficiency. In addition, this bearing can be adapted to various applications with the use of cages that are targeted for specific work environments or conditions.

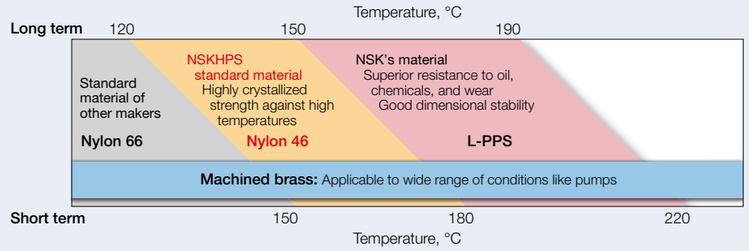

Fig. 2 Features and heat resistance of cage materials

Table 3 Bearing table

Bore diameter (mm)	Bearing No.	Basic load rating (N)				Limiting speed (rpm)	
		NSKHPS		Standard bearing		NSKHPS	Standard bearing
		C_r	C_{0r}	C_r	C_{0r}		
12	7201B (EA)	8 150	3 750	7 450	3 750	30 000	26 000
	7301B (EA)	11 100	4 950	8 850	4 200	26 000	22 000
15	7202B (EA)	9 800	4 800	7 950	4 300	26 000	22 000
	7302B (EA)	14 300	6 900	12 500	6 600	22 000	19 000
17	7203B (EA)	11 600	6 100	9 950	5 500	22 000	19 000
	7303B (EA)	16 800	8 300	14 800	8 000	20 000	17 000
20	7204B (EA)	15 600	8 150	13 300	7 650	19 000	16 000
	7304B (EA)	19 800	10 500	17 300	9 650	18 000	15 000
25	7205B (EA)	17 600	10 200	14 800	9 400	17 000	14 000
	7305B (EA)	27 200	14 900	24 400	14 600	15 000	13 000
30	7206B (EA)	23 700	14 300	20 500	13 500	14 000	12 000
	7306B (EA)	36 500	20 600	31 000	19 300	13 000	11 000
35	7207B (EA)	32 500	19 600	27 100	18 400	12 000	10 000
	7307B (EA)	40 500	24 400	36 500	24 200	11 000	9 500
40	7208B (EA)	38 500	24 500	32 000	23 000	11 000	9 000
	7308B (EA)	53 000	33 000	45 000	30 500	10 000	8 500
45	7209B (EA)	40 500	27 100	36 000	26 200	10 000	8 500
	7309B (EA)	62 500	39 500	58 500	40 000	9 000	7 500
50	7210B (EA)	42 000	29 700	37 500	28 600	9 500	8 000
	7310B (EA)	78 000	50 500	68 000	48 000	8 000	6 700
55	7211B (EA)	51 500	37 000	46 500	36 000	8 500	7 100
	7311B (EA)	89 000	58 500	79 000	56 500	7 500	6 300
60	7212B (EA)	61 500	45 000	56 000	44 500	7 500	6 300
	7312B (EA)	102 000	68 500	90 000	65 500	6 700	5 600
65	7213B (EA)	70 000	53 500	63 500	52 500	7 100	6 000
	7313B (EA)	114 000	77 000	102 000	75 500	6 300	5 300
70	7214B (EA)	75 500	58 500	69 000	58 000	6 700	5 600
	7314B (EA)	124 000	87 500	114 000	86 000	6 000	5 000
75	7215B (EA)	78 500	63 500	68 500	58 500	6 300	5 300
	7315B (EA)	134 000	98 500	125 000	97 500	5 600	4 800
80	7216B (EA)	87 500	70 000	80 500	69 500	6 000	5 000
	7316B (EA)	144 000	110 000	135 000	109 000	5 300	4 300

Low-Torque, Highly Rigid, Thin-Section, Angular Contact Ball Bearings Fitted with Outer Seals

In a wide range of industries such as the medical treatment, biotechnology, optical component, and automobile industries, there is a growing need to improve precision and efficiency of factory automation (FA) devices. In the actuators of handling and transfer systems or machine tools, and the joints of industrial robots, direct drive (DD) motors that enable highly precise positioning are becoming more widely used instead of gears. Bearings for all of these applications are thus required to operate with even lower torque and higher rigidity.

Responding to these needs, NSK has developed and commercialized a low-torque, highly rigid, thin-section, angular contact ball bearings fitted with outer seals (Photo 1).

Photo 1 Low-torque, highly rigid, thin-section, angular contact ball bearings fitted with outer seals

1. Structure and Specifications

Figure 1 illustrates a cutaway view of the low-torque, highly rigid, thin-section, angular contact ball bearing fitted with outer seals. This newly developed bearing has been designed with optimal internal specifications, is packed with highly fretting-resistant grease, and sealed with highly functional, compact, non-contact rubber seals mounted to both sides of the bearing.

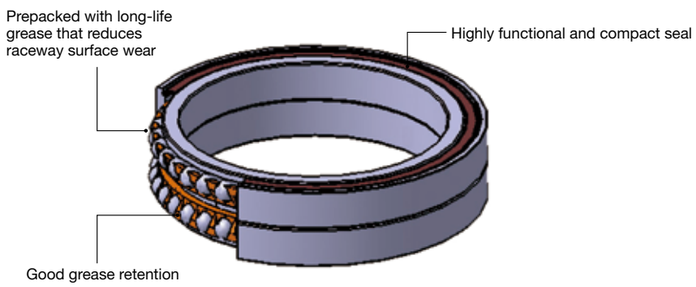

Fig. 1 Structure of low-torque, highly rigid, thin-section, angular contact ball bearing fitted with outer seals

2. Features

Features of the low-torque, highly rigid, thin-section, angular contact ball bearing fitted with outer seals are described as below.

(1) Achieves a higher degree of precision and conserves energy through low-torque performance and minimal torque fluctuations

At present, transport devices, positioning tables, and industrial robots primarily use crossed roller bearings. NSK has successfully reduced starting torque by 50 % and dynamic torque by up to 75 %, compared with crossed roller bearings, by employing balls as the rolling elements (Figures 2 and 3), which results in reduced energy consumption. Additionally, torque fluctuations are kept to a minimum, which results in improved positioning accuracy.

(2) Saves space by offering both a compact design and high load capacity

NSK has optimized the number and diameter of the balls used in the bearing to ensure rigidity and load capacity equal to or greater than that of the crossed roller bearing. As a result, the outer diameter dimensions of the bearing have been reduced by up to 30 %.

(3) Achieves maintenance-free performance by means of a longer operating life

The bearing is packed with highly fretting-resistant grease and sealed with non-contact rubber seals. An improved plastic cage that retains grease well and is highly heat resistant was also developed. As a result, operating life is approximately six times longer than that of a conventional crossed roller bearing.

3. Summary

By adopting this newly developed bearing, end-user equipment and devices can benefit from a higher degree of precision, reduced energy consumption, a compact design, and maintenance-free performance.

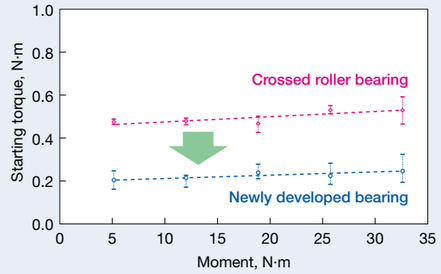

Newly developed bearing: 50 mm bore, 65 mm outside diameter, 14 mm width
Crossed roller bearing: 50 mm bore, 80 mm outside diameter, 13 mm width

Fig. 2 Comparison of starting torque

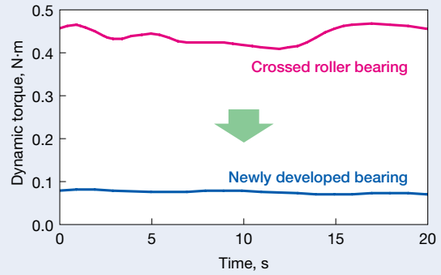

Newly developed bearing: 50 mm bore, 65 mm outside diameter, 14 mm width
Crossed roller bearing: 50 mm bore, 80 mm outside diameter, 13 mm width

Fig. 3 Comparison of dynamic torque

General-Purpose, Shielded Deep Groove Ball Bearings with High Load Capacity

Bearings that are used under heavy load conditions are increasingly required to provide higher bearing load ratings to meet the need for longer bearing life. However, enlarging bearings may be difficult due to limited space inside machinery, or there may be a need to avoid increased frictional loss associated with larger bearings in order to reduce energy consumption. To this end, NSK has commercialized a general-purpose, shielded deep groove ball bearing with high load capacity and offers excellent features that meet the aforementioned needs.

1. Structure and Specifications

Bearing internal structure was reassessed; resulting in a maximum 26 % improvement in basic dynamic load rating compared with conventional bearings. In addition, the shape of the shield was also redesigned to combine high load capacity performance and sealing performance, which until now was difficult to achieve.

Photo 1 General-purpose, shielded deep groove ball bearings with high load capacity

2. Features

(1) Longer life under heavy load conditions

Dynamic load rating was improved by a maximum of 26 % compared with bearings of the same size by using the maximum number of balls with larger diameters (Figure 1). This development extends bearing service life by a maximum of twofold compared with conventional bearings (Figure 2).

(2) Thin shield

A new thin shield was developed to accommodate balls with an extra large diameter, and to provide good sealing performance, while maintaining the same size as that of a conventional bearing but with higher load capacity (Figure 3).

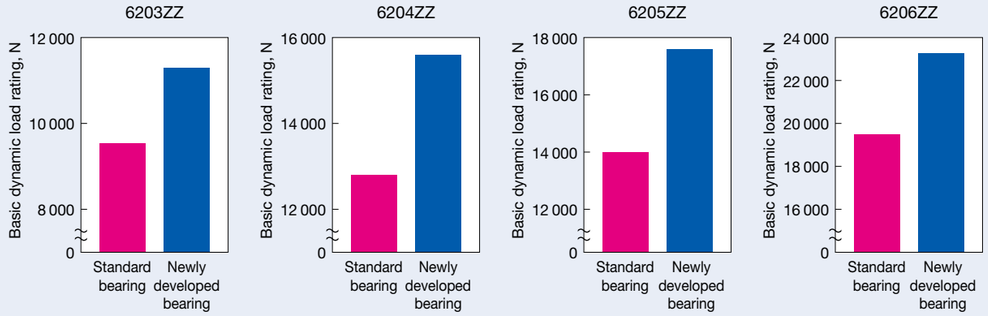

Fig. 1 Comparison of basic dynamic load ratings

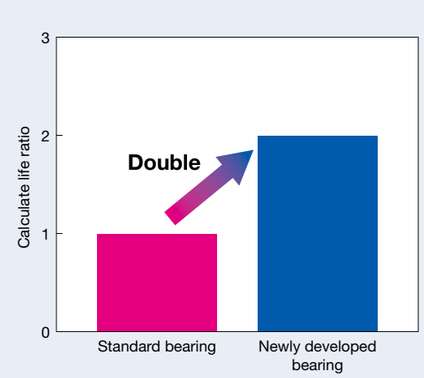

Fig. 2 Comparison of rating fatigue life

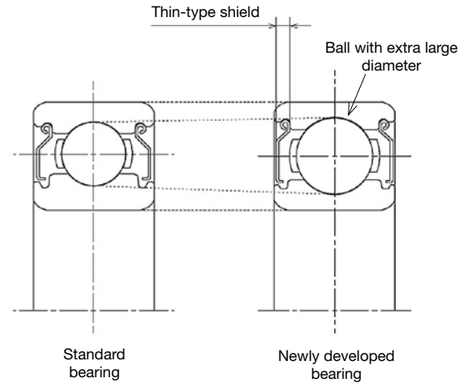

Fig. 3 Cross-sectional comparison of a standard bearing and the newly developed bearing

3. Interchangeable with Conventional Bearings

Boundary dimensions of this newly developed bearing are the same as ISO-standard bearings of the same size, which facilitates easy retrofitting of current applications.

4. Applications

This newly developed bearing is suitable for applications requiring high load capacity, such as motor reduction gears, industrial pumps, agricultural equipment, and drum-type washing machines.

5. Summary

We have introduced a newly developed, general-purpose, shielded deep groove ball bearing with higher load capacity and longer life for use under heavy load conditions. We will continue efforts to further progress with developments that respond to the various needs of users.

Highly Reliable & Long-Life Split Cylindrical Roller Bearing Units for Segmented Drive Rolls

Recent years have seen growing demand for heavy steel plate that is used in shipbuilding and energy-production industries. In a continuous casting machine, there is a tendency towards higher loads in the production process of larger slabs. Consequently, support rolls used in this production process require bearings that can meet the demand for load-carrying capacity performance. Meanwhile, due to the need for maintaining a cleaner operating environment, oil-air lubrication has been adopted or methods of collecting waste grease have been used extensively.

NSK has newly developed a highly reliable and long-life Split Cylindrical Roller Bearing Unit for segmented drive rolls (Photo 1) to respond to these needs. This bearing unit has an improved internal design as well as adopting a new type of seal, and offers higher load-carrying capacity and is capable of accommodating various lubrication methods.

Photo 1 Highly reliable & long-life Split Cylindrical Roller Bearing Unit

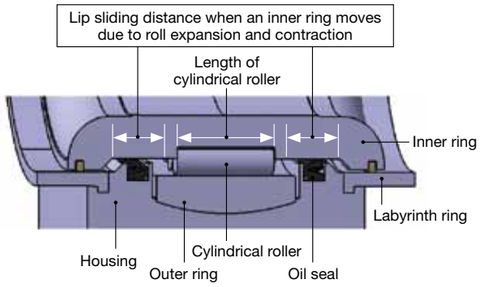

Fig. 1 Cutaway view of a conventional product

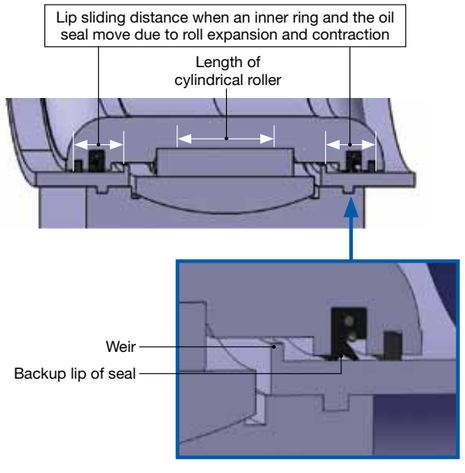

Fig. 2 Cutaway view of the newly developed product

1. Structure and Features

(1) Long life

The oil seal of conventional split-cylindrical roller bearing units (Figure 1) is mounted to the outer ring and has a seal lip that maintains sliding contact with the inner ring outside surface. At the same time, due to high-temperature slabs coming into contact with the drive rolls during operation, the drive roll repeatedly expands and contracts due to thermal expansion. During expansion and contraction of the roll, the inner ring is also moved in the axial direction. Consequently, the contact point between the seal lip and the inner ring outside surface moves according with the movement of the inner ring. In order to maintain the amount of axial space during movement, the width of the inner ring raceway surface was limited, which prevented the use of longer cylindrical rollers.

At this time, the newly developed Split Cylindrical Roller Bearing Unit (Figure 2) has an oil seal, which is an outer circumference seal, that is mounted to the inner ring so that the seal lip slides on the labyrinth ring bore surface. Accordingly, width of the inner ring raceway surface is not affected by axial movement resulting from roll expansion and contraction. Thus, the new internal design is able to accommodate a wider amount of space for cylindrical rollers. As a result, this newly developed bearing unit offers 30 % longer cylindrical rollers and achieves twice the service life in comparison with a conventional cylindrical roller bearing unit.

(2) Cleaner working conditions

By adopting a structure with a “weir” as a labyrinth, the initially supplied oil lubricant in the bearing interior is sufficiently maintained. Thus, this newly developed Split Cylindrical Roller Bearing Unit is able to use oil-air lubrication systems that have gained wider attention in recent years. Furthermore, this bearing unit adopts a highly reliable oil seal with backup lip in case of grease lubrication in order to reduce leakage from the bearing unit, and is able to address the issue of waste grease collection.

Adopting these structures enables the use of oil-air lubrication and the prevention of grease leakage from the bearing unit in the case of grease lubrication, and ensures cleaner operating conditions around the continuous casting machine.

2. Configuration and Dimensions

Table 1 lists typical examples of the specifications for NSK’s highly reliable and long-life Split Cylindrical Roller Bearing Units for segmented drive rolls.

3. Summary

NSK’s highly reliable and long-life Split Cylindrical Roller Bearing Units for segmented drive rolls for continuous casting machines offer extended bearing life, which helps prevent sudden bearing failure and reduces maintenance costs. This product also functions as an environmentally conscious product in that it contributes to a cleaner operating environment.

Table 1 Specifications of Split Cylindrical Roller Bearing Units

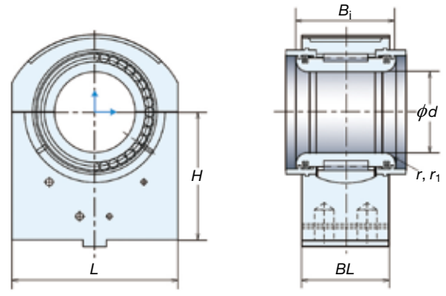

Unit: mm

Caster roll O. D.	Roll neck		Bearing number		Basic load rating (kN)		Boundary dimensions					Permitted axial displacement
	Width BL	Fillet radius r_1	Housing	Bearing	C_r	C_{0r}	d	B_i	r	L	H	
210	155	18	100RCPH171	100PHR211	405	950	100	154	18	200	145	10
220	140	15	110RCPH181	110PHR221	450	1 090	110	139	15	220	225	9
225	155	20	110RCPH193	110PHR233	500	1 200	110	154	20	230	180	10
230	138	15	110RCPH191	110PHR231	480	1 120	110	137	15	230	160	8
235	158	20	120RCPH201	120PHR231	540	1 340	120	157	20	234	165	8
240	174	15	115RCPH201	115PHR241	600	1 400	115	173	15	240	220	6
250	184	20	135RCPH211	135PHR251	515	1 350	135	183	20	250	160	10
255	180	20	120RCPH216	120PHR256	630	1 580	120	179	20	255	230	8
260	185	20	140RCPH221	140PHR261	565	1 410	140	184	20	260	185	10.5
265	192	20	140RCPH223	140PHR263	615	1 570	140	191	20	265	250	6
270	180	20	140RCPH231	140PHR271	665	1 750	140	179	20	270	245	6
280	197	20	145RCPH233	145PHR283	675	1 800	145	196	20	280	250	10
295	209	20	150RCPH251	150PHR291	754	1 870	150	208	20	295	310	6
300	200	20	155RCPH251	155PHR301	770	1 970	155	199	20	300	260	8
310	185	20	140RCPH261	140PHR311	840	1 970	140	184	20	310	175	9
320	201	20	160RCPH281	160PHR331	1 070	2 650	160	200	20	330	225	7
330	236	25	170RCPH281	170PHR331	1 100	2 870	170	235	25	330	280	6
335	170	20	180RCPH291	180PHR331	780	1 800	180	169	20	335	217.5	8
340	236	25	180RCPH281	180PHR341	980	2 490	180	235	25	340	280	6
370	234	20	190RCPH331	190PHR391	1 510	3 850	190	233	20	390	280	6

TW Series of Ball Screws for Twin-Drive Systems

Ball screws are widely used as a drive system component in machine tools including electric injection molding machines, semiconductor manufacturing equipment, robots, conveyors, food processing equipment, and medical equipment. Based on in-house research conducted at the Japan International Machine Tool Fair in 2006, NSK concluded that the number of high-speed machine tools with a feed rate of 50 to 60 meters per minute has been increasing for use in machining centers. Additionally, together with the high-speed feed rates, demands for greater rigidity of feed systems are increasing.

The number of the twin-drive systems, in which two ball screws are used for a single table, has been increasing in order to achieve higher-speed feed rates, and higher-rigidity and higher-accuracy. NSK has commercialized the TW series of ball screws and offers a lineup of this new series, which is the best type of ball screws for these twin-drive systems (Photo 1).

Photo 1 TW series of ball screws for twin-drive systems

1. Specifications

Types of ball recirculation methods:	middle-deflector type (HMD), tube type, deflector type (bridge type)
Screw shaft diameter:	32 mm to 63 mm
Lead:	10 mm to 30 mm
Accuracy grade:	JIS C5
Screw shaft length:	3 m or less
Optional specifications:	JIS grade C3, hollow shaft ball screw*

(*Available upon request to enhance accuracy performance using forced cooling.)

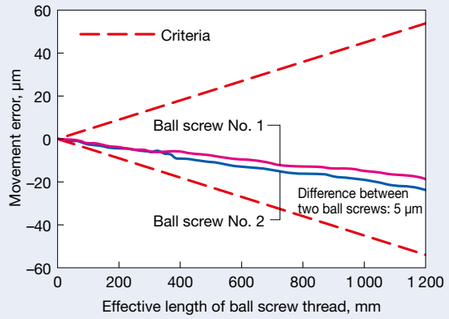

Fig. 1 Example of measured variations in lead accuracy for two ball screws

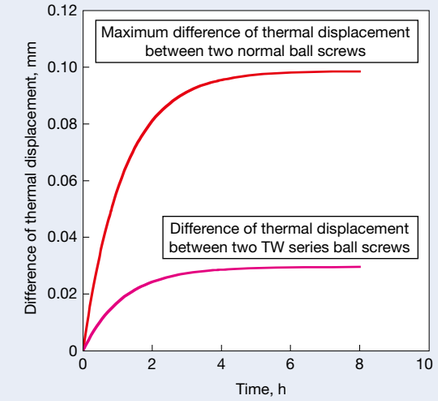

Specifications and conditions of ball screws
Shaft diameter: 40 mm
Lead: 20 mm
Torque: 51 N·cm to 106 N·cm
Stroke: 1 000 mm
Maximum rotational speed: 3 000 rpm
Average rotational speed: 230 rpm

Fig. 2 Example of calculated difference of thermal displacement between two ball screws in a system

2. Features

The TW series is a special ball screws for twin-drive systems consisting of two ball screws and two motors mounted to a single-shaft feed mechanism. Compared with a conventional single-drive system using one ball screw, the diameter of the screw shaft can be made smaller resulting in less inertia acting on the motor, which facilitates faster acceleration and deceleration cycles.

Additionally, permissible rotational speed can be increased and faster maximum feed rates can be achieved with the smaller shaft diameter of the ball screw. With two ball screws with smaller shaft diameters, greater rigidity of the whole system and the shaft can be achieved when compared with the conventional single ball screw with a large diameter.

(1) Highly accurate feeding

The mutual differences of dynamic torque due to preload and lead accuracy between the two ball screws of the TW series are controlled within certain restrictions. Thus, the deterioration of mechanical accuracy and the reduction of service life, resulting from the difference of axial displacement between two ball screws, are suppressed in the application of the TW series, though two ball screws are used together side-by-side.

Figure 1 shows measured variations in lead accuracy of two TW series ball screws and the difference between those two ball screws. Figure 2 illustrates the difference of thermal displacements for two TW series ball screws and that for two normal ball screws. Thermal displacements are calculated using dynamic torques due to preload. Figure 3 illustrates a comparison of travel accuracy between the TW series and normal ball screws.

(2) Quiet running

When two ball screws are used side-by-side, ball screw noise levels rise by approximately 3 dB theoretically compared with a single ball screw. However, the rise in noise level of the newly developed TW series is almost none because of smaller shafts. Using a middle-deflector type (HMD) recirculation circuit enables quieter low-noise operation.

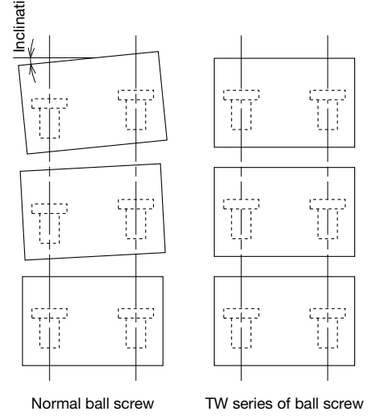

Fig. 3 Comparative drawings of travel accuracy

3. Applications

This series of ball screws is suitable for machining centers, multi-axis and multifunctional machines, and larger processing machines.

HMD Series of Ball Screws for High-Speed Machine Tools

Against the backdrop of demand for improved efficiency in industries, machine tools that perform at increasingly higher speeds are making much progress. Based on research conducted by NSK, Figure 1 shows the trend of rapid traverse speeds of machining centers that were on display at the Japan International Machine Tool Fair (JIMTOF). Machines with a rapid traverse speed of 60 m/min, which in general have been emblematic of high-speed machines, have continued to increase since beginning our research. The maximum speed of the machines has been as high as 120 m/min.

Accordingly, ball screws used for feed drive systems in these machine tools have required higher speeds. However, conventional measures using return tubes had the problem of increasing tube costs or deteriorating sound and vibration characteristics.

Therefore, NSK fundamentally reviewed the conventional recirculation method, and developed the BSS series of ball screws, resulting in both significantly higher speeds and greater noise reduction. NSK has received high marks for the BSS series of ball screws in transportation and handling equipment for industries.

NSK has commercialized the HMD series of ball screws for high-speed machine tools by applying to machine tools the high-speed and quiet-running technologies cultivated from the development of the BSS series.

Photo 1 HMD series of ball screws for high-speed machine tools

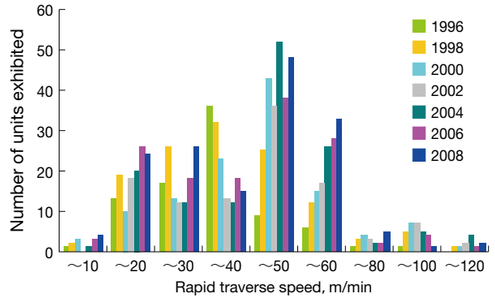

Fig. 1 Trend of rapid traverse speeds of machining centers at JIMTOF

1. Structure and Specifications

The BSS series features a smooth ball circulation mechanism using a component called an end deflector. This component has helped the BSS series to achieve unparalleled increasing of limiting speed and exceptional improvement of low sound and low vibration characteristics. Because end deflectors were placed at both ends of the nut, however, the recirculation circuit had basically one row, and preloading was accomplished with oversized-ball preload.

Meanwhile, ball screws for machine tools are mostly required to have offset lead preload, which necessitates more than one independent recirculation circuit in the nut. Such a requirement restricted the application of the BSS series to the ball screws for use in machine tools.

NSK addressed this issue with a newly developed middle deflector and the recirculation method using it. In this new recirculation circuit, the balls are smoothly scooped from the ball screw groove at the middle point of the nut by the middle deflector, which therefore enables the use of more than just one independent recirculation circuit in the nut. This development helped to bring about the HMD series of high-speed and quiet-running ball screws with offset lead preload (Figure 2).

2. Features

(1) High-speed performance

High-speed and quiet-running technology (Figure 3), in which matching the direction of the scoop in the recirculation circuit with the tangential direction of the screw is a key point, has resulted in achieving a permissible $d{\cdot}n$ value (shaft diameter × rotational speed) of 160 000.

For example, a ball screw with a 40 mm shaft diameter and a 20 mm lead is capable of an 80 m/min feed rate at 4 000 rpm of high-speed rotation. In addition, if a 30 mm lead ball screw is used, it is possible to increase the feed rate up to 120 m/min. Thus, the HMD series can contribute to higher efficiency in machine tools with these levels of performance.

(2) Low noise

Because impact between the balls and recirculation components is absorbed by means of the high-speed and quiet-running technology, noise levels have been reduced by 6 dB (Figure 4).

For example, the noise levels of the HMD series

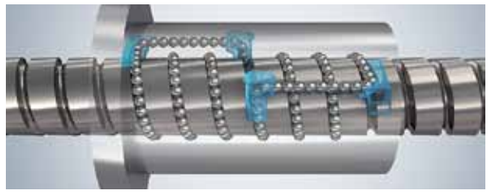

Fig. 2 Internal view of the HMD series showing the ball recirculation circuit

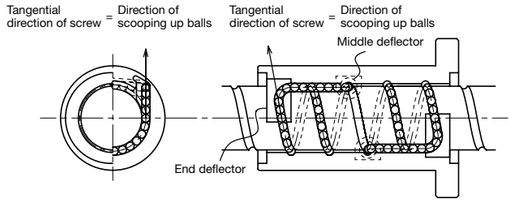

Fig. 3 Key points of the HMD series for achieving high-speed and quiet-running performance

operating at a speed 4 000 rpm is equal to the level of noise in a conventional ball screw operating at 2 400 rpm. The typical amount of increased noise levels under high-speed rotation due to increased limiting speeds is fully compensated by the successful application of this significant achievement in noise reductions.

(3) High rigidity and high load-carrying capacity

By using special specifications of the ball groove for machine-tool applications, rigidity has been increased by threefold and loading capacity has been increased by twofold in comparison with NSK's standard product.

In addition, because permissible $d{\cdot}n$ value (shaft diameter × rotational speed) has been increased, it is possible to use a larger shaft diameter (d) as long as the rotational speed (n) remains the same. If the current application is using ball screws with a shaft diameter of 40 mm at 3 000 rpm, for example, it is possible to use ball screws with a shaft diameter by up to 50 mm. This improves axial rigidity by nearly twofold, which contributes to more highly accurate positioning. Although it is not widely known that improved permissible $d{\cdot}n$ value leads to such a significant improvement in higher rigidity, such an improvement can have a significantly positive impact on designing in rigidity-focused feed systems.

(4) Compact

NSK has focused on the development of manufacturing technologies of the ball screw nuts, which has resulted in the processing and manufacturing of a ball screw nut that exceed the previous fabricating limitation of nut length. The full lineup of the HMD series feature offset lead preload by application of these technologies and the newly developed recirculation circuit using the middle deflector.

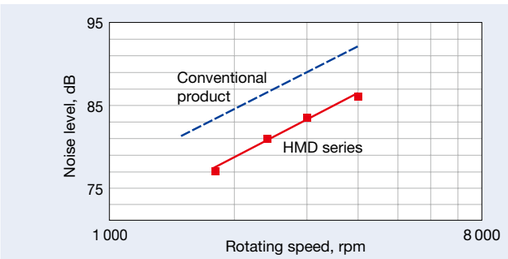

Fig. 4 Comparison of noise levels

Table 1 Lineup and maximum feed rate

Unit: m/min

Shaft diameter (mm) \ Lead (mm)	16	20	25	30
40	64	80	100	120
45	56	71	88	—
50	51	64	80	96
63	40	—	—	—

Thus, the ball nut length is shortened by a maximum 20 % in the case of conventionally used ball screws with double nut preload. This contributes to downscaling machine tools and expanding the processing range of machine tools.

(5) Wealth of options

The following options are provided in response to various demands that are unique to machine tools:

- Ball screw specifications for twin drive applications
- Ball screw specifications with a hollow shaft for shaft-core cooling
- Ball screw specifications for vertical axis applications

Further details are available in NSK Catalog No. 3236.

3. Specifications

Table 1 lists the maximum feed rates for available specifications. Twelve types of ball screws are available with shaft diameters of 40 mm through 63 mm and leads of 16 mm through 30 mm.

4. Applications

This series is suitable for high-speed machine tools from among machine tools such as machining centers, turning centers, and multi-axis/multifunctional machines.

5. Summary

The HMD series will further expand the current lineup to include smaller sizes and larger sizes. NSK expects to further develop this series of ball screws for a wider range of machine tools in the future.

RB Series Roller Guides of NSK Linear Guides

NSK developed the RA series of roller guides in 2003 in response to demands for linear guides that offer greater functionality (longer life and higher rigidity) for use in machine tool applications. The RA series achieved the world's highest loading capacity and rigidity and has acquired a favorable reputation in the marketplace.

In recent years, as manufacturing equipment of liquid crystal display panels became larger and machine tools with multi-functional and multi-spindle designs increased, these machines have increased demand for designs that are more compact, are more highly rigid, and have a lower center of gravity, resulting in increased demand for linear guides that provide a lower assembly height.

In response to these demands, NSK has developed the RB series of ultralow-profile roller guides (Photo 1).

The RB series of roller guides feature a significant reduction in assembly height while maintaining features of super high loading capacity and super high rigidity of the RA series of roller guides that are being used throughout a wide range of fields. The RB series thus contributes to further downscaling, lowering the center of gravity, and promoting higher rigidity in applications and equipment.

1. Features

Development of the RB series, which was based on the RA series, offers the following features:

(1) Maximum 26 % reduction in assembly height

By enabling the downscaling and lowering the center of gravity of equipment, improving equipment rigidity and reducing load on the linear guides became achievable (Photo 2).

Photo 1 RB series of roller guides

(2) World's highest rigidity and loading capacity

Optimization of rolling element contact conditions has been achieved by incorporating internal dimensions that take into consideration deformation of roller slide itself. In addition, dimensions of internal components (raceway surface and rollers) have the same specifications as those of the RA series, thus ensuring the same degree of high rigidity and high loading capacity.

(3) Improved fretting resistance

Fretting resistance has been improved by using rollers with minimal differential sliding. Thus the RB series is most suitable for applications or operating conditions where minute movements are repeated.

(4) Highly dust resistant and long-term maintenance free performance

End seals, inner seals, and bottom seals are equipped as standard to prevent ingress of foreign matter. Furthermore, an upper rail cover is available as an option for use in severe environments.

Additionally, the RB series can be equipped with the NSK K1 lubrication unit, which has a long and positive history with NSK linear guides.

2. Specifications

Table 1 lists model numbers and types of roller slides prepared for the RB series. In addition, Table 2 lists main boundary dimensions of rectangle-type roller slides as representative examples.

(1) Shape and dimensions

- Assembly height has been lowered by a maximum of 26 % compared with the conventional LH series, LA series, and RA series.
- Mounting tap holes on the flanged-type roller slide can be used as through holes, and allow users to secure the roller slide from both upper or lower sides.
- Six types for RB55 and five types for RB65 are available with differing mounting hole positions on the roller slide. Retrofitting with this series can be easily implemented without changing the machine design as is the case with general ultralow-type ball guides.

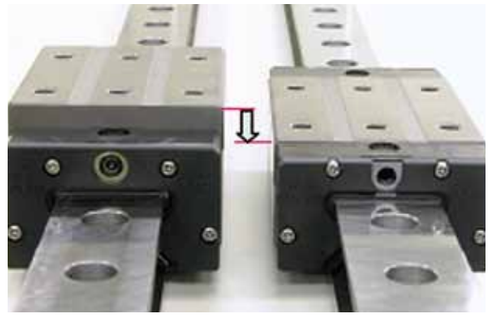

RA45 RB45

Photo 2 Assembly-height comparison of RA series and RB series

(2) Accuracy and preload

- Four types of accuracy grades are available: ultra precision P3, super precision P4, high precision P5, and precision grade P6.
- Only the middle preload type is available because differences in rigidity between the differing preloads is small and high rigidity can be stably obtained from the characteristics of the roller guide.

Table 1 Model numbers and types of roller slides

Model numbers	Types of roller slides					
	Rectangle high-load type		Rectangle super-high-load type		Flanged type	
	AL	TL	BL	UL	EM	GM
RB30	○	—	○	—	○	○
RB35	○	—	○	—	○	○
RB45	○	—	○	—	○	○
RB55	○	○	○	○	○	○
RB65	○	—	○	○	○	○

3. Applications

The RB series of roller guides contributes to downscaling and lowering of the center of gravity for equipment while maintaining rigidity and service life. This series is most suitable for increasingly larger machine tools because of multifunctional/multi-spindle, and for conveyor robots used in liquid crystal display panel manufacturing facilities handling panels that have grown in size.

4. Summary

NSK has commercialized the RB series of roller guides to help promote downscaling and to enable the lowering of the center of gravity of equipment. NSK will hereafter promote the expansion of this series by improving various functions for our customers in using roller guides with further expanded applications.

Table 2 Specifications of RB series of roller guides (rectangle type)

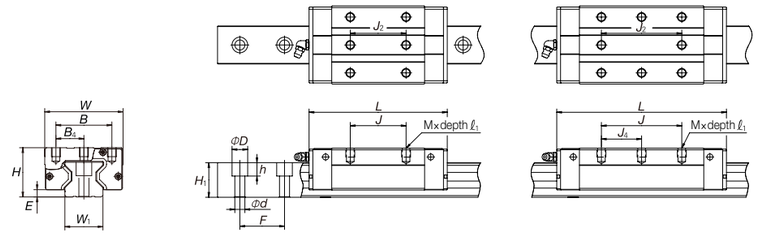

Rectangle high-load type (AL, TL)

Rectangle super-high-load type (BL, UL)

Unit: mm

Model No.	Assembly		Roller slide									Rail				Basic load rating				
	Height		Width	Length	Mounting hole						Nipple mounting hole	Width	Height	Pitch	Mounting hole	Dynamic load rating	Static load rating	Static moment (N·m)		
	H	E	W	L	B	B4	J	J2	J4	No. of mounting hole	M×ℓ1		W1	H1	F	d×D×h	C (N)	C0 (N)	MR0	MP0	MY0
RB30AL	38	6.5	60	110.8	40	20	40	40	—	6	M8×7	3	28	28	40	9×14×12	38 900	93 500	1 670	1 140	1 140
RB30BL				135.4			60	60	30	8							47 600	121 000	2 170	1 950	1 950
RB35AL	44	6.5	70	123.8	50	25	50	50	—	6	M8×8	M6×0.75	34	31	40	9×14×12	53 300	129 000	2 810	1 800	1 800
RB35BL				152			72	72	36	8							67 400	175 000	3 810	3 250	3 250
RB45AL	52	8	86	154	60	30	60	60	—	6	M10×10	M6×0.75	45	38	52.5	14×20×17	92 800	229 000	6 180	4 080	4 080
RB45BL				190			80	80	40	8							116 000	305 000	8 240	7 150	7 150
RB55AL	63	9	100	184	65	—	75	—	—	4	M12×12	Rc1/8	53	43.5	60	16×23×20	129 000	330 000	10 200	7 060	7 060
RB55TL					75	37.5		75		6											
RB55BL				234	65	—	95	95	47.5								168 000	462 000	14 300	13 600	13 600
RB55UL					75	37.5			—												
RB65AL	75	10	126	228.4	76	38	70	70	—	6	M16×16	Rc1/8	63	52	75	18×26×22	210 000	504 000	19 200	12 700	12 700
RB65BL				302.5		—	110	—	55								288 000	756 000	28 700	28 600	28 600
RB65UL						38	120	120	—												

*Locations of roller slide mounting holes are different between RB55AL and RB55TL, and between RB55BL and RB55UL.
*Locations of roller slide mounting holes are different between RB65BL and RB65UL.

Worldwide Sales Offices

P: Phone F: Fax ☆: Head Office

NSK LTD.-HEADQUARTERS, TOKYO, JAPAN

Nissei Bldg., 1-6-3 Ohsaki, Shinagawa-ku, Tokyo 141-8560, Japan

INDUSTRIAL MACHINERY BUSINESS DIVISION-HEADQUARTERS
P: +81-3-3779-7227 F: +81-3-3779-7644

AUTOMOTIVE BUSINESS DIVISION-HEADQUARTERS
P: +81-3-3779-7189 F: +81-3-3779-7917

●Africa

South Africa:

NSK SOUTH AFRICA (PTY) LTD.

JOHANNESBURG 25 Galaxy Avenue, Linbro Business Park, Sandton, Gauteng, P.O. Box 1157, Kelvin, 2054, South Africa
P: +27-11-458-3600 F: +27-11-458-3608

●Asia and Oceania

Australia:

NSK AUSTRALIA PTY. LTD.

MELBOURNE ☆ 11 Dalmore Drive, Scoresby, Victoria 3179, Australia
P: +61-3-9765-4400 F: +61-3-9764-8304

SYDNEY 24-28 River Road West, Parramatta, New South Wales 2150, Australia
P: +61-2-8843-8100 F: +61-2-9893-8406

BRISBANE 1/69 Selhurst Street, Coopers Plains, Queensland 4108, Australia
P: +61-7-3347-2600 F: +61-7-3345-5376

PERTH Unit 1, 71 Tacoma Circuit, Canning Vale, Western Australia 6155, Australia
P: +61-8-9256-5000 F: +61-8-9256-1044

New Zealand:

NSK NEW ZEALAND LTD.

AUCKLAND 3 Te Apunga Place, Mt. Wellington, Auckland, New Zealand
P: +64-9-276-4992 F: +64-9-276-4082

China:

NSK HONG KONG LTD.

HONG KONG ☆ Suite 705, 7th Floor, South Tower, World Finance Centre, Harbour City, T.S.T, Kowloon, Hong Kong, China
P: +852-2739-9933 F: +852-2739-9323

SHENZHEN Room 624-626, 6/F, Kerry Center, Renminnan Road, Shenzhen, Guangdong, China
P: +86-755-25904886 F: +86-755-25904883

NSK (SHANGHAI) TRADING CO., LTD.

JIANGSU No.8 NSK Rd., Huaqiao Economic Development Zone, Kunshan, Jiangsu, China (215332)
P: +86-512-5796-3000 F: +86-512-5796-3300

NSK (CHINA) INVESTMENT CO., LTD.

JIANGSU ☆ No.8 NSK Rd., Huaqiao Economic Development Zone, Kunshan, Jiangsu, China (215332)
P: +86-512-5796-3000 F: +86-512-5796-3300

BEIJING Room 2116, Beijing Fortune Bldg., 5 Dong San Huan Bei Lu, Chao Yang District, Beijing, China (100004)
P: +86-10-6590-8161 F: +86-10-6590-8166

TIAN JIN Room 06, 09F The Exchange Tower 2, No. 189 NanJing Road, Heping District, Tianjin, China (300050)
P: +86-22-8319-5030 F: +86-22-8319-5033

CHANGCHUN Room 1001, Building A, Zhongyin Building, 727 Xi'an Road, Changchun, Jilin, China (130061)
P: +86-431-8898-8682 F: +86-431-8898-8670

SHENYANG Room 1101, China Resources Building, No. 286 Qingnian Street, Heping District, Shenyang Liaoning, China (110004)
P: +86-24-2334-2868 F: +86-24-2334-2058

DALIAN Room 1805 Xiwang Tower, No.136 Zhongshan Road, Zhongshan District, Dalian, Liaoning, China (116001)
P: +86-411-8800-8168 F: +86-411-8800-8160

NANJING Room A1 22F, Golden Eagle International Plaza, No.89 Hanzhong Road, Nanjing, Jiangsu, China (210029)
P: +86-25-8472-6671 F: +86-25-8472-6687

FUZHOU Room 1801-1811, B1#1A Class Office Building, Wanda Plaza, No.8 Aojiang Road, Fuzhou, China (350009)
P: +86-591-8380-1030 F: +86-591-8380-1225

WUHAN Room 2108, New World International Trade Tower I, No.568 Jianshe Road, Wuhan, Hubei, China (430000)
P: +86-27-8556-9630 F: +86-27-8556-9615

QINGDAO Room 802, Farglory International Plaza, No.26 Xianggang Zhong Road, Shinan District, Qingdao, Shandong, China (266071)
P: +86-532-5568-3877 F: +86-532-5568-3876

GUANGZHOU Room 2302, TaiKoo Hui Tower 1, No.385 Tianhe Road, Tianhe District, Guangzhou, China (510620)
P: +86-20-3817-7800 F: +86-20-3786-4501

CHANGSHA Room 1048, 10/F, Zhongtian Plaza, No.766 WuyiRoad, Changsha, Hunan, China (410005)
P: +86-731-8571-3100 F: +86-731-8571-3255

LUOYANG Room 1108, Fangda Hotel, 6 XiYuan Road, LuoYang HeNan, China (471003)
P: +86-379-6069-6188 F: +86-379-6069-6180

XI'AN Room 1007, B Changan Metropolls Center88 Nanguanzheng Steet, Xi'an, Shanxi, China (710068)
P: +86-29-8765-1896 F: +86-29-8765-1895

CHONGQING Room 2306, Unit B, No.137, Keyuan 2nd Road, Jiulongpo District, Chonqing, China (400039)
P: +86-23-6806-5310 F: +86-23-6806-5292

CHENGDU Room1117, Lippo Tower, No.62 North Kehua Road, Chengdu, Sichuan, China (610041)
P: +86-28-8528-3680 F: +86-28-8528-3690

NSK CHINA SALES CO., LTD.

JIANGSU No.8 NSK Rd., Huaqiao Economic Development Zone, Kunshan, Jiangsu, China (215332)
P: +86-512-5796-3000 F: +86-512-5796-3300

India:

NSK INDIA SALES CO.PVT.LTD.

CHENNAI ☆ 6th Floor, Bannari Amman Towers, No.29 Dr. Radhakrishnan Salai, Mylapore, Chennai-600 004 Tamil Nadu, India
P: +91-44-2847-9600 F: +91-44-2847-9601

GURGAON Unit No-202, 2nd Floor, Block-A, Iris Tech Park, Sector-48, Gurgaon, Haryana-122008, India
P: +91-124-4104-530 F: +91-124-4104-532

KOLKATA 502, Trinity Towers, 83, Topsia Road, Kolkata-700 046, India
P: +91-33-4001-2062 F: +91-33-4001-2064

MUMBAI 321, 'A' Wing, Ahura Centre, 82, Mahakali Caves Road, Andheri (East), Mumbai -400 093, India
P: +91-22-2838-7787 F: +91-22-2838-5191

Indonesia:

PT. NSK INDONESIA

JAKARTA Summitmas II, 6th Floor, Jl. Jend Sudirman Kav. 61-62, Jakarta 12190, Indonesia
P: +62-21-252-3458 F: +62-21-252-3223

Korea:

NSK KOREA CO., LTD.

SEOUL Posco Center (West Wing) 9F, 892, Daechi-4Dong, Kangnam-Ku, Seoul, 135-777, Korea
P: +82-2-3287-0300 F: +82-2-3287-0345

Malaysia:

NSK BEARINGS (MALAYSIA) SDN. BHD.

SHAH ALAM ☆ No. 2, Jalan Pemaju, U1/15, Seksyen U1, Hicom Glenmarie Industrial Park, 40150 Shah Alam, Selangor, Malaysia
P: +60-3-7803-8859 F: +60-3-7806-5982

PRAI No.36, Jalan kikik, Taman Inderawasih, 13600 Prai, Penang, Malaysia
P: +60-4-3902275 F: +60-4-3991830

JOHOR BAHRU 88 Jalan Ros Merah 2/17, Taman Johor Jaya, 81100 Johor Bahru, Johor, Malaysia
P: +60-7-3546290 F: +60-7-3546291

IPOH Gr. Floor, 89 Jalan Bendahara, 31650 Ipoh, Perak, Malaysia
P: +60-5-2555000 F: +60-5-2553373

Philippines:

NSK REPRESENTATIVE OFFICE

MANILA 8th Floor The Salcedo Towers 169 H.V. dela Costa St., Salcedo Village Makati City, Philippines 1227
P: +63-2-893-9543 F: +63-2-893-9173

Singapore:

NSK INTERNATIONAL (SINGAPORE) PTE LTD.

SINGAPORE 238A, Thomson Road, #24-01/05, Novena Square Tower A, Singapore 307684
P: +65-6496-8000 F: +65-6250-5845

NSK SINGAPORE (PRIVATE) LTD.

SINGAPORE 238A, Thomson Road, #24-01/05, Novena Square Tower A, Singapore 307684
P: +65-6496-8000 F: +65-6250-5845

Taiwan:

TAIWAN NSK PRECISION CO., LTD.

TAIPEI ☆ 11F., No.87, Song Jiang Rd., Jhongshan District, Taipei City 104, Taiwan R.O.C.
P: +886-2-2509-3305 F: +886-2-2509-1393

TAICHUNG 107-7, Sec. 3, Wen Xing Rd., Taichung City 407, Taiwan R.O.C.
P: +886-4-2311-7978 F: +886-4-2311-2627

TAINAN 5F. No.8, Daye 1st Rd., Southern Taiwan Science Park, Tainan City 741, Taiwan R.O.C.
P: +886-6-505-5861 F: +886-6-505-5061

TAIWAN NSK TECHNOLOGY CO., LTD.

TAIPEI ☆ 11F., No.87, Song Jiang Rd., Jhongshan District, Taipei City 104, Taiwan R.O.C.
P: +886-2-2509-3305 F: +886-2-2509-1393

TAICHUNG 10F-3, No.123, Sec.3, Junggang Rd., Taichung 407, Taiwan R.O.C.
P: +886-4-2358-2945 F: +886-4-2358-7682

TAINAN 5F. No.8, Daye 1st Rd., Southern Taiwan Science Park, Tainan City 741, Taiwan R.O.C.
P: +886-6-505-5861 F: +886-6-505-5061

Thailand:

NSK BEARINGS (THAILAND) CO.,LTD.

BANGKOK 26 Soi Onnuch 55/1 Pravet Subdistrict, Pravet District, Bangkok 10250, Thailand
P: +66-2320-2555 F: +66-2320-2826

Vietnam:

NSK VIETNAM CO., LTD.

HANOI Techno Center, Room 204-205, Thang Long Industrial Park, Dong Anh District, Hanoi, Vietnam
P: +84-4-3955-0159 F: +84-4-3955-0158

NSK REPRESENTATIVE OFFICE

HO CHI MINH CITY Suite 307, Metropolitan Building, 235 Dong Khoi Street, District 1,HCMC, Vietnam
P: +84-8-3822-7907 F: +84-8-3822-7910

Worldwide Sales Offices

P: Phone F: Fax ☆: Head Office

●Europe

United Kingdom:

NSK EUROPE LTD. (EUROPEAN HEADQUARTERS)

MAIDENHEAD Belmont Place, Belmont Road, Maidenhead, Berkshire SL6 6TB, U.K.
P: +44-1628-509-800 F: +44-1628-509-808

NSK UK LTD.

NEWARK Northern Road, Newark, Nottinghamshire NG24 2JF, U.K.
P: +44-1636-605-123 F: +44-1636-605-000

France:

NSK FRANCE S.A.S.

PARIS Quartier de l'Europe, 2 Rue Georges Guynemer, 78283 Guyancourt, France
P: +33-1-30-57-39-39 F: +33-1-30-57-00-01

Germany:

NSK DEUTSCHLAND GMBH

DUSSELDORF ☆ Harkortstrasse 15, D-40880 Ratingen, Germany
P: +49-2102-4810 F: +49-2102-4812-290

STUTTGART Liebknechtstrasse 33, D-70565 Stuttgart-Vaihingen, Germany
P: +49-711-79082-0 F: +49-711-79082-289

WOLFSBURG Tischlerstrasse 3, D-38440 Wolfsburg, Germany
P: +49-5361-27647-10 F: +49-5361-27647-70

Italy:

NSK ITALIA S.P.A.

MILANO Via Garibaldi 215, Garbagnate Milanese (Milano) 20024, Italy
P: +39-299-5191 F: +39-299-025778

Norway:

NSK EUROPE NORWEGIAN BRANCH NUF

SANDEFIJORD Østre Kullerød 5, N-3241 Sandefjord, Norway
P: +47-33-293160 F: +47-33-429002

Netherlands:

NSK EUROPEAN DISTRIBUTION CENTRE B.V.

TILBURG De Kroonstraat 38, 5048 AP Tilburg, Netherlands
P: +31-13-4647647 F: +31-13-4647648

Poland:

NSK REPRESENTATIVE OFFICE

WARSAW Ul. Migdalowa 4/73, 02-796, Warsaw, Poland
P: +48-22-645-1525 F: +48-22-645-1529

Russia:

NSK POLSKA SP. Z O.O.

SAINT-PETERSBURG Office I 703, Bldg 29, 18th Line of Vasilievskiy Ostrov, Saint-Petersburg, Russia, 199178
P: +7-812-332-5071 F: +7-812-332-5072

Spain:

NSK SPAIN S.A.

BARCELONA C/Tarragona 161, 2a Planta, 08014, Barcelona, Spain
P: +34-93-433-5775 F: +34-93-433-5776

Turkey:

NSK RULMANLARI ORTA DOGU TIC. LTD. STI.

ISTANBUL 19 Mayis Mah. Ataturk Cad. Ulya Engin Is Merkezi No. 68 Kat. 6, Kozyatagi 34734, Istanbul, Turkey
P: +90-216-355-0398 F: +90-216-355-0399

UAE:

NSK BEARINGS GULF TRADING CO.

DUBAI JAFZA View 19, Floor 24 Office 2/3 Jebel Ali Downtown, PO Box 262163, Dubai, UAE
P: +971-4-804-8200 F: +971-4-884-7227

●North and South America

United States of America:

NSK AMERICAS, INC. (AMERICAN HEADQUARTERS)

ANN ARBOR 4200 Goss Road, Ann Arbor, Michigan 48105, U.S.A.
P: +1-734-913-7500 F: +1-734-913-7511

NSK CORPORATION

ANN ARBOR 4200 Goss Road, Ann Arbor, Michigan 48105, U.S.A.
P: +1-734-913-7500 F: +1-734-913-7511

NSK PRECISION AMERICA, INC.

FRANKLIN ☆ 3450 Bearing Drive, Franklin, Indiana 46131, U.S.A.
P: +1-317-738-5000 F: +1-317-738-5050

SAN JOSE 780 Montague Expressway, Suite 508, San Jose, California 95131, U.S.A.
P: +1-408-944-9400 F: +1-408-944-9405

NSK LATIN AMERICA, INC.

MIAMI 2500 NW 107th Avenue, Suite 300, Miami, Florida 33172, U.S.A.
P: +1-305-477-0605 F: +1-305-477-0377

Canada:

NSK CANADA INC.

TORONTO ☆ 5585 McAdam Road, Mississauga, Ontario, Canada L4Z 1N4
P: +1-905-890-0740 F: +1-800-800-2788

MONTREAL 2150-32E Avenue Lachine, Quebec, Canada H8T 3H7
P: +1-514-633-1220 F: +1-800-800-2788

VANCOUVER 3353 Wayburne Drive, Burnaby, British Columbia, Canada V5G 4L4
P: +1-877-994-6675 F: +1-800-800-2788

Argentina:

NSK ARGENTINA SRL

BUENOS AIRES Garcia del Rio 2477 Piso 7 Oficina "A" (1429) Buenos Aires-Argentina
P: +54-11-4704-5100 F: +54-11-4704-0033

Brazil:

NSK BRASIL LTDA.

SAO PAULO ☆ Rua 13 de Maio, 1633-14th Andar-Bela Vista-CEP 01327-905 São Paulo, SP, Brazil
P: +55-11-3269-4786 F: +55-11-3269-4720

BELO HORIZONTE Rua Ceara 1431-4th andar-sala 405-Funcionarios Belo Horizonte-MG, Brazil 30150-311
P: +55-31-3274-2591 F: +55-31-3273-4408

JOINVILLE Rua Blumenau, 178-sala 910-Centro Joinville-SC, Brazil 89204-250
P: +55-47-3422-5445 F: +55-47-3422-2817

PORTO ALEGRE Av. Cristovão Colombo, 1694-sala 202-Floresta Porto Alegre-RS, Brazil 90560 001
P: +55-51-3222-1324 F: +55-51-3222-2599

RECIFE Av. Conselheiro Aguiar, 2738-6th andar-conj. 604-Boa Viagem Recife-PE, Brazil 51020-020
P: +55-81-3326-3781 F: +55-81-3326-5047

Peru:

NSK PERU S.A.C.

LIMA Av. Caminos del Inca 670, Ofic : # 402, Santiago del Surco, Lima, Perú
P: +51-1-652-3372 F: +51-1-638-0555

Mexico:

NSK RODAMIENTOS MEXICANA, S.A. DE C.V.

MEXICO CITY ☆ Av. Presidente Juarez No.2007 Lote 5, Col. San Jeronimo Tepetlacalco, Tlalnepantla, Estado de Mexico, Mexico, C.P.54090
P: +52-55-3682-2900 F: +52-55-3682-2937

MONTERREY Av. Ricardo Margain 575, IOS Torre C, Suite 516, Parque Corporativo Santa Engracia, San Pedro Garza Garcia, N.L. Mexico, C.P.66267
P: +52-81-8000-7300 F: +52-81-8000-7095

<As of April 2013>

For the latest information, please refer to the NSK website.
www.nsk.com

Motion & Control

No. 23 June 2013

Published by NSK Ltd.

Eco-awareness and reliability in motion

NSK

NSK used environmentally friendly printing methods for this publication.

CAT. No. ETJ-0023 2013 C-6 Printed in Japan